



Shaw, J. M., Evenstar, L., Cooper, F. J., Adams, B. A., Boyce, A., Hofmann, F., & Farley, K. (2021). A rusty record of weathering and groundwater movement in the hyperarid Central Andes. *Geochemistry, Geophysics, Geosystems*, 22(8), [e2021GC009759]. <https://doi.org/10.1029/2021GC009759>

Publisher's PDF, also known as Version of record

License (if available):
CC BY

Link to published version (if available):
[10.1029/2021GC009759](https://doi.org/10.1029/2021GC009759)

[Link to publication record in Explore Bristol Research](#)
PDF-document

This is the final published version of the article (version of record). It first appeared online via AGU at <https://doi.org/10.1029/2021GC009759>. Please refer to any applicable terms of use of the publisher.

University of Bristol - Explore Bristol Research

General rights

This document is made available in accordance with publisher policies. Please cite only the published version using the reference above. Full terms of use are available: <http://www.bristol.ac.uk/red/research-policy/pure/user-guides/ebr-terms/>

Geochemistry, Geophysics, Geosystems



RESEARCH ARTICLE

10.1029/2021GC009759

Key Points:

- Hematite (U-Th-Sm)/He weathering geochronology constrains late Miocene exhumation rates in the Atacama Desert of northern Chile
- Hematite records prolonged post-hyperaridity development of weathering profiles in the Atacama Desert
- Exhumation is the most important driver of relative water table descent during supergene enrichment of porphyry copper deposits

Supporting Information:

Supporting Information may be found in the online version of this article.

Correspondence to:

J. M. Shaw,
joseph.shaw@bristol.ac.uk





Citation:

Shaw, J. M., Evenstar, L., Cooper, F. J., Adams, B. A., Boyce, A. J., Hofmann, F., & Farley, K. A. (2021). A rusty record of weathering and groundwater movement in the hyperarid Central Andes. *Geochemistry, Geophysics, Geosystems*, 22, e2021GC009759. <https://doi.org/10.1029/2021GC009759>

Received 9 MAR 2021

Accepted 14 JUL 2021

A Rusty Record of Weathering and Groundwater Movement in the Hyperarid Central Andes

J. M. Shaw¹ , L. Evenstar² , F. J. Cooper¹, B. A. Adams¹, A. J. Boyce³ , F. Hofmann⁴ , and K. A. Farley⁴

¹School of Earth Sciences, University of Bristol, Bristol, UK, ²School of Environment and Technology, University of Brighton, Brighton, UK, ³Scottish Universities Environmental Research Centre, East Kilbride, UK, ⁴Division of Geological and Planetary Sciences, California Institute of Technology, Pasadena, CA, USA

Abstract The Atacama Desert, on the western margin of the Central Andes, hosts some of the world's largest porphyry copper deposits (PCDs). Despite a hyperarid climate, many of these PCDs have undergone secondary “supergene” enrichment, whereby copper has been concentrated via groundwater-driven leaching and reprecipitation, yielding supergene profiles containing valuable records of weathering and landscape evolution. We combine hematite (U-Th-Sm)/He geochronology and oxygen isotope analysis to compare the weathering histories of two Andean PCDs and test the relative importance of climate and tectonics in controlling both enrichment and water table movement. At Cerro Colorado, in the Precordillera, hematite precipitation records prolonged weathering from ~31 to ~2 Ma, tracking water table descent following aridity-induced canyon incision from the late Miocene onward. By contrast, hematite at Spence, within the Central Depression, is mostly younger than ~10.5 Ma, suggesting exhumation ended much later. A heavy oxygen isotopic signature for Spence hematite suggests that upwelling formation water has been an important source of groundwater, accounting for a high modern water table despite persistent hyperaridity, whereas isotopically light hematite at Cerro Colorado formed in the presence of meteoric water. Compared with published paleo-environmental and sedimentological records, our data show that weathering can persist beneath appreciable post-exhumation cover, under hyperarid conditions unconducive to enrichment. The susceptibility of each deposit to aridity-induced water table descent, canyon incision and deep weathering has been controlled by recharge characteristics and morphotectonic setting. Erosional exhumation, rather than aridity-induced water table decay, appears to be more important for the development of supergene enrichment.

Plain Language Summary Northern Chile hosts many large copper deposits which were formed at depths of several kilometers and then brought close to the surface during Andean mountain-building. Water-driven weathering reactions have upgraded some exhumed deposits by leaching copper from sulfide minerals under oxidizing conditions and reprecipitating it within new minerals under reducing conditions, in a process called supergene (“from above”) enrichment. Relative water table descent is required for these processes to expand into fresh ore, but it is unclear whether climatic or tectonic factors have been more important controls on water table movement in different locations. In this study, we investigate the age and oxygen isotopic composition of the iron oxide weathering mineral, hematite, from the supergene profiles of two Andean copper deposits (Spence and Cerro Colorado) to constrain and compare the timing of weathering and sources of weathering fluids. The preserved record of weathering begins at ~31 Ma at Cerro Colorado but the main period of weathering at Spence occurred after ~10.5 Ma. Oxygen isotopes show that differing responses of the water table to increased aridity after the late Miocene (descending at Cerro Colorado but remaining shallow at Spence) have depended on catchments, groundwater flow, and differences in topography.

1. Introduction

The Central Andes of northern Chile host many large porphyry copper deposits (PCDs)—hydrothermally generated, sulfide-bearing orebodies centered on felsic to intermediate igneous intrusions (Richards, 2013). Initially formed at depths of ~1–4 km (Sillitoe, 2010), many PCDs have been exhumed to the (near-)surface following the late Eocene Incaic orogeny (Riquelme et al., 2018). The economic metal concentrations of some exhumed PCDs were produced during weathering, via meteoric water-driven “supergene” (from

© 2021. The Authors.

This is an open access article under the terms of the [Creative Commons Attribution](https://creativecommons.org/licenses/by/4.0/) License, which permits use, distribution and reproduction in any medium, provided the original work is properly cited.

above) enrichment, whereby copper is leached from sulfide minerals undergoing oxidation at, or above, the water table and concentrated below the water table via processes of dissolution, solution transport, and reprecipitation (Chávez, 2000; Sillitoe, 2005; Sillitoe & McKee, 1996). For weathering and enrichment to progress, tectonic or climatic factors must trigger relative water table descent for fresh rock to be exposed to oxidation and leaching (Ague & Brimhall, 1989; Alpers & Brimhall, 1988; Anderson, 1982; Brimhall et al., 1985). This could be caused by uplift of rock through the water table (Sillitoe, 2005) (hereon referred to as “*exhumation-driven water table descent*,” where the water table is the reference datum), or climate-induced canyon incision or reduction in aquifer recharge (Cooper et al., 2016), lowering the water table (hereon referred to as “*water table decay*,” where the surface is the reference datum). Understanding of the relative contribution of these factors to water table movement during the development of preserved weathering profiles is limited (García et al., 2011), and as mineral deposits become harder to find, greater knowledge of the controls on paleo-water tables in different settings will be essential for future exploration.

Previous studies have constrained the timing of enrichment of Andean PCDs via K-Ar and $^{40}\text{Ar}/^{39}\text{Ar}$ dating of supergene alunite group minerals; K-bearing sulfates formed as by-products of sulfide leaching (Alpers & Brimhall, 1988; Arancibia et al., 2006; Bouzari & Clark, 2002; Sillitoe & McKee, 1996). A major limitation on the usefulness of alunite is that it can form under oxidising conditions above the water table (Sillitoe & McKee, 1996) and under reducing conditions beneath it (Alpers & Brimhall, 1988), implying that samples separated by hundreds of meters within a weathering profile may have formed “anytime from several million years apart to synchronously” (Sillitoe, 2005). Therefore, a more redox-sensitive indicator mineral is required to understand the relationship between water tables, enrichment, and the development of PCD weathering profiles, and identify controls on water table movement and groundwater flow in a tectonically and climatically dynamic area.

Iron oxides, such as hematite (Fe_2O_3), are common authigenic weathering minerals and can be dated using (U-Th-Sm)/He geochronology, providing a tool for constraining periods of weathering (Monteiro et al., 2014) and tracking water table movement (Cooper et al., 2016; Deng et al., 2017; Heim et al., 2006), as these minerals, and their metastable precursors, predominantly form under oxygenated conditions at or above the atmosphere-groundwater interface (Heim et al., 2006). The only application of hematite (U-Th-Sm)/He geochronology to an Andean PCD weathering profile, which tracked water table decay at Cerro Colorado in the Andean Precordillera (Figure 1) was conducted by Cooper et al. (2016). Here, geochronology data show that weathering had commenced by ~ 31 Ma and persisted until at least ~ 2 Ma. An apparent younging-with-depth trend observed after 16 Ma was attributed to aridity-induced incision of a nearby canyon (the Quebrada de Parca) which continues to control the local water table today. These geochronology data show that regional climate can control water table movement and the progression of weathering via canyon incision, and that hematite precipitation persisted long after supergene enrichment ended (at ~ 14.6 Ma; Bouzari & Clark, 2002), suggesting that hematite is not a proxy for enrichment. However, the response of the water table in different locations to desiccation of the Atacama Desert, and the impacts of this response on the supergene development of different PCDs are yet to be determined.

This contribution re-examines the history of canyon incision and water table decay at Cerro Colorado (based on satellite imagery of truncated drainage networks and published ages of volcanic deposits contained within the gravel cover proximal to the deposit), and investigates the timing of weathering at Spence, an enriched PCD situated within the Central Depression, ~ 300 km south. In contrast to Cerro Colorado, Spence has not been affected by canyon incision and the modern water table is shallow despite persistent hyperaridity (Cameron & Leybourne, 2005). We report oxygen isotopic measurements ($\delta^{18}\text{O}$) for Fe-oxides from the weathering profiles at Spence and Cerro Colorado, enabling recharge mechanisms and groundwater sources during weathering to be constrained and compared.

2. Background

2.1. PCD Formation and Supergene Enrichment in the Central Andes

PCDs are typically located within arc-parallel belts at convergent plate boundaries, such as the western Andean margin of South America, where magmatism, PCD formation and orogenesis have resulted from subduction of the Farallon and Nazca plates beneath the South American plate from the mid to late Jurassic

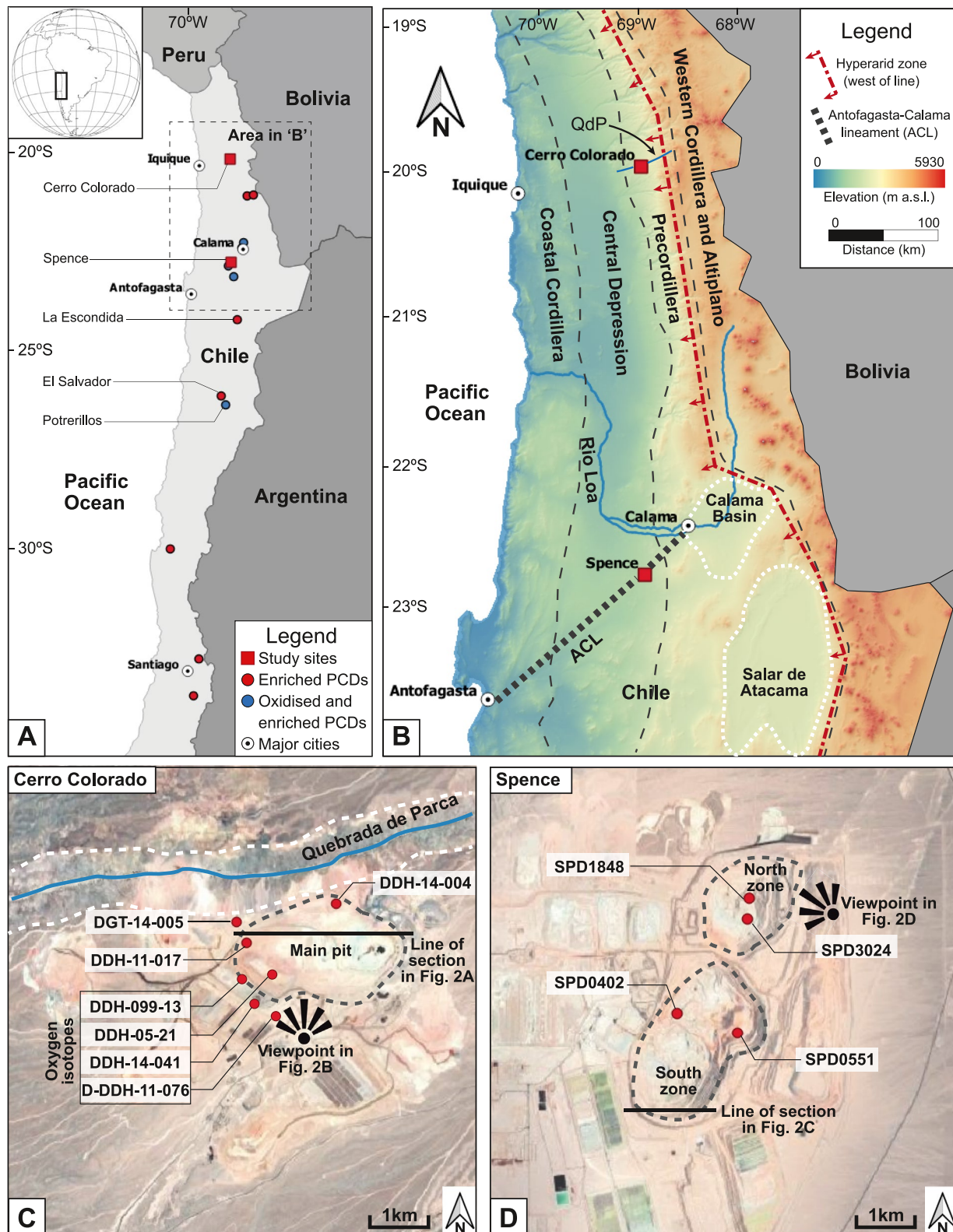


Figure 1. (a) Locations of Central Andean porphyry copper deposits discussed in the text, color coded according to enrichment type. Dashed box encompasses the study area in (b). (b) Elevation map of northern Chile showing locations of Cerro Colorado and Spence. Dashed black lines separate the morphotectonic units of the western Andean margin. Dashed red line marks the eastern limit of the hyperarid core of the Atacama Desert. (c and d) Google Earth™ views of Cerro Colorado and Spence showing locations and IDs of sampled drill holes (red circles).

onward (Armijo et al., 2015; Mpodozis & Cornejo, 2012; Richards, 2013; Sillitoe, 2010). PCDs form when heat and water expulsion from stocks and dykes, emplaced above granitoid plutons at paleo-depths of several kilometers, drive hydrothermal alteration of large volumes of rock and generate disseminated and vein-hosted sulfide mineralization (e.g., pyrite [FeS₂] and chalcopyrite [CuFeS₂]; Sillitoe, 2010).

Erosional exhumation has brought many PCDs to the near-surface, where copper present in hypogene (*“formed from below”*) orebodies may be concentrated by up to a factor of three by supergene processes (Sillitoe, 2005). In the supergene environment, Cu enrichment is produced via chemical weathering by descending meteoric waters. Oxidation of sulfides at or above the water table forms sulfuric acid, enabling downward leaching of Cu. Under reducing conditions, beneath the water table, Cu is reprecipitated, forming enriched secondary sulfides (e.g., chalcocite [Cu₂S] and covellite [CuS]; Ague & Brimhall, 1989; Sillitoe, 2005). Where acidity or water availability are insufficient for leaching, in situ oxidation may produce an “oxide zone” containing secondary Cu minerals such as atacamite and brochantite (Sillitoe, 2005; Vasconcelos, 1999). Mature supergene weathering profiles thus comprise an upper, weathered zone, underlain by a sulfide enrichment blanket grading downward into the hypogene orebody. The boundary between the weathered zone and enrichment blanket represents the deepest paleo-water table position—the “ultimate redox front.”

Although there is evidence supergene enrichment is most effective during periods of landscape stability, characterized by pediplanation and low erosion rates (Riquelme et al., 2018; Sanchez et al., 2018), sufficient lowering of the water table for deep weathering is aided by periods of tectonic uplift (Sillitoe, 2005). Between 26° and 27°S, the deeply leached and strongly enriched El Salvador deposit, which experienced multiple phases of tectonic uplift and erosion during the Oligocene and middle Miocene, contrasts with the Potrerillos deposit, which is less deeply exhumed and hosts a less mature supergene profile (Bissig & Riquelme, 2009). This shows the relative importance of climatic and tectonic factors and the extent to which they affect water tables are spatially variable.

Many Andean PCDs are buried beneath Miocene gravels which form regionally extensive paleo-surfaces (Evenstar et al., 2017; Hollingworth, 1964). Cover deposition may end enrichment by stopping precipitation reaching the water table, especially in areas with low infiltration rates and high evapotranspiration such as the Atacama (Davis et al., 2010). Furthermore, burial may cause the ultimate redox front to be “drowned” beneath an elevated water table, so that infiltrating water is moving through rocks already leached of copper (Brimhall et al., 1985; Enders et al., 2006; Sillitoe & McKee, 1996). Ages of paleo-surfaces and ash layers within gravel units allow PCD weathering ages to be viewed within a sedimentological framework of pre-versus post-cover deposition (Bouzari & Clark, 2002).

2.2. Central Andean Neogene Paleoclimate

The western Andean margin of South America comprises five arc-parallel morphotectonic units; the Coastal Cordillera, Central Depression, Precordillera, Western Cordillera and Altiplano (Barnes & Ehlers, 2009; Figure 1). Encompassing much of the Coastal Cordillera, Central Depression, and Precordillera, between 15° and 30°S at elevations of 0–3,500 m a.s.l., the hyperarid core of the Atacama Desert is one of the driest places on Earth (Amundson et al., 2012; Bookhagen & Strecker, 2012; Garreaud et al., 2010; Houston, 2006a, 2006b; Houston & Hartley, 2003; Sun et al., 2018). Despite this, the region hosts many PCDs that have been enriched by meteoric groundwater (Arancibia et al., 2006; Hartley & Rice, 2005; Sillitoe, 2005).

Hyperaridity in the Atacama Desert is sustained by its latitudinal location within the Inter-Tropical Convergence Zone, the cold Humboldt ocean current moving northward along the west coast of South America, its distance from the Atlantic Ocean, and the effect of the Andean rain shadow, which blocks moisture from the Amazon basin (Houston, 2006b; Houston & Hartley, 2003). Modern mean annual rainfall (MAR) at Cerro Colorado is 20 mm (Jordan et al., 2014) and Spence receives <10 mm (Sun et al., 2018). Estimates for the onset of hyperaridity range from Oligocene (Dunai et al., 2005) to Pliocene (Hartley & Rice, 2005), although it is generally considered to have begun during the middle to late Miocene. Evidence for strengthening aridity in the middle Miocene includes the apparent cessation of PCD supergene enrichment at ~14 Ma (Alpers & Brimhall, 1988; Sillitoe & McKee, 1996), and increasingly heavy oxygen isotopic compositions of soil carbonates by 15 Ma (Rech et al., 2019). How-

ever, multiple sedimentological and isotopic records indicate climate desiccation, from (semi-)arid to hyperarid conditions, in the late Miocene, between ~ 12 and ~ 10 Ma, due to a strengthening of the Andean rain shadow (Rech et al., 2019). Gypsum-cemented (“gypcrete”) horizons, formed when MAR was < 20 mm, are preserved beneath ~ 9.5 Ma ignimbrites in the Precordillera and Central Depression (Hartley & May, 1998; Jordan et al., 2014; Rech et al., 2019). Similarly, non-reworked soluble salt horizons in the gravels covering Spence, preserved beneath a 9.47 ± 0.04 Ma ash layer (Sun et al., 2018), suggest precipitation has been insufficient for direct recharge since this time. Isotopic evidence for hyperaridity includes increasingly heavy $\delta^{18}\text{O}$ and $\delta^{13}\text{C}$ signatures in palustrine carbonates in the Calama Basin after 12 Ma (Rech et al., 2010) and higher $\delta^{18}\text{O}$ in travertine deposits at Barrancos Blancas (24°S) after ~ 11.5 Ma (Quade et al., 2017). Global datasets suggest that direct recharge is negligible when MAR is < 200 mm (Houston, 2009; Scanlon et al., 2006). Therefore, it is unlikely that either Cerro Colorado or Spence have experienced direct recharge since the onset of hyperaridity, especially through volcanic and sedimentary cover. Instead, indirect recharge by precipitation higher in the Andes and deep formation water (saline porewaters and meteoric water with a long residence time) are likely contributors to groundwater at lower elevations in the Precordillera and Central Depression (Hoke et al., 2004; Houston, 2002; Magaritz et al., 1990).

2.3. Weathering and Water Tables at Cerro Colorado and Spence

Comparing Cerro Colorado and Spence is useful because, despite their similar hypogene mineralization ages (53.5–50 Ma at Cerro Colorado [Bouzari & Clark, 2002; Tsang et al., 2018] and ~ 57 Ma at Spence [Rowland & Clark, 2001]), subsequent exhumation, weathering, and water table movement at each deposit have operated under contrasting tectonic, sedimentological, and geomorphological conditions.

At Cerro Colorado, situated 2,600 m a.s.l. within the Andean Precordillera (Figures 1 and 2), (U-Th-Sm)/He hematite ages record persistent weathering from early Oligocene to Pleistocene (~ 31 –2 Ma; Cooper et al., 2016). By comparison, $^{40}\text{Ar}/^{39}\text{Ar}$ alunite ages suggest the onset of supergene enrichment was coeval at ~ 35 Ma but ceased in the middle Miocene at ~ 14.6 Ma (Bouzari & Clark, 2002). A minimum age for the end of exhumation is provided by the 19.25 ± 0.43 Ma Tambillo ignimbrite, which covers much of the deposit (Bouzari & Clark, 2002), ruling out regional, exhumation-driven water table descent as the cause of the post-middle Miocene water table decay observed by Cooper et al. (2016). Cover deposition at Cerro Colorado, represented by gravels of the El Diablo Formation, continued until ~ 11 Ma (Blanco et al., 2012), when climate desiccation led to surface abandonment (Evenstar et al., 2017) and decreased river discharge led to channel steepening and incision of the Quebrada de Parca (Cooper et al., 2016).

Spence lies within the Central Depression, at 1,700 m a.s.l., along the Antofagasta-Calama Lineament (ACL), a SW-NE-striking crustal-scale fracture which facilitated magma emplacement during formation of the deposit (Palacios et al., 2007) (Figures 1 and 2). Unpublished alunite ages suggest Spence was enriched between ~ 44 and ~ 21 Ma (Rowland & Clark, 2001), although it is unclear whether all dated samples were of supergene origin. Spence is covered by 50–100 m of Atacama Gravels (Cameron & Leybourne, 2005). A 9.47 ± 0.04 Ma ash layer, situated 37 m above the gravel-bedrock contact, provides a minimum age for the end of exhumation (Sun et al., 2018) (Figures 2a and 2b). Unlike at Cerro Colorado, which is cut by the Quebrada de Parca, the nearest river is the Rio Loa, 34 km to the north (Figure 1b). Although it has been suggested that Spence lies within the groundwater catchment of the Rio Loa (Jordan et al., 2015), the water table slopes toward the southwest (Cameron & Leybourne, 2005). Furthermore, the Rio Loa did not breach the Coastal Cordillera until the late Pliocene to late Pleistocene, shifting the river base level from $> 1,000$ m a.s.l. in the Central Depression to sea level at the Pacific Ocean, and causing upstream channel incision (May et al., 2005; Ritter et al., 2018). Incision of the Rio Loa is therefore unlikely to have influenced the water table at Spence. In contrast to Cerro Colorado, the modern water table at Spence is elevated relative to the ultimate redox front, approximating the gravel-bedrock contact, despite persistent hyperaridity. Oxygen isotope analysis of local groundwater suggests this is caused by upwelling formation water along the ACL, which acts as a fluid pathway for deep groundwater recharge (Cameron & Leybourne, 2005).

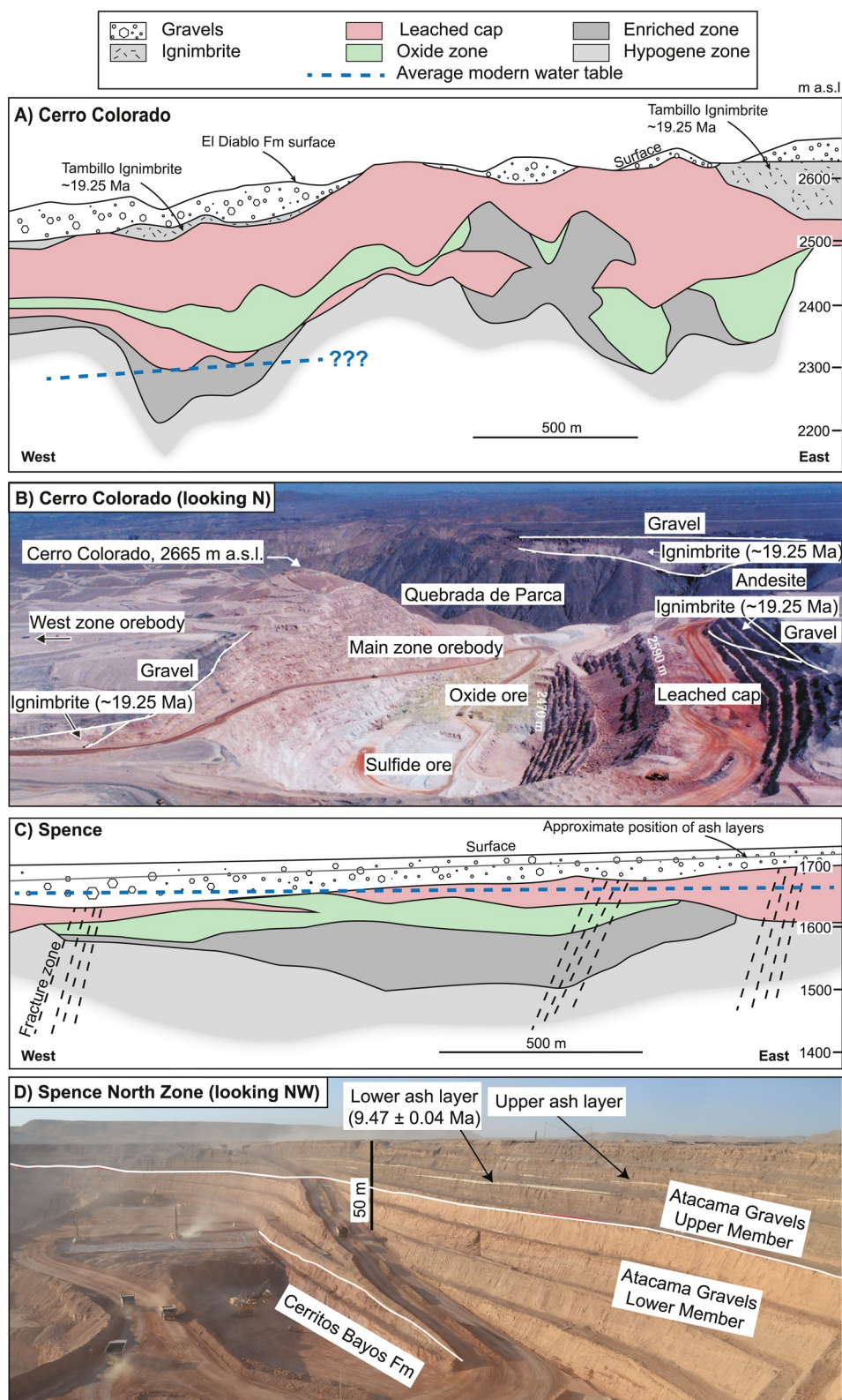
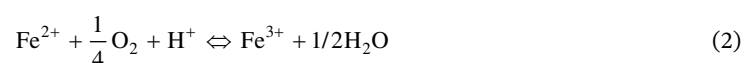
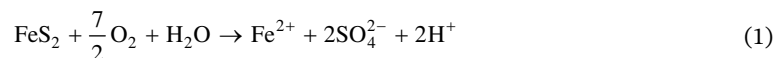


Figure 2.

2.4. Hematite as a Record of Water Table Movement and Weathering Fluid Composition

Fe-oxide formation during PCD weathering is thought to be caused by oxidation of sulfides at or above the water table (Ague & Brimhall, 1989), with minor sub-water table sulfide oxidation along high-permeability pathways (Lichtner & Biino, 1992). For pyrite, the summary reactions are approximated below (Dold, 2003):



Sulfide oxidation (Equation 1) requires free oxygen, sourced either from the atmosphere or from oxygenated groundwater. In arid areas with low permeability and slow-moving groundwater, such as our study sites, this limits efficient weathering to the unsaturated zone, at or above the water table. Oxygen involved in subsequent Fe-oxide precipitation is primarily contributed by water (Equations 2 and 3), enabling the isotopic composition, and source, of groundwater during Fe-oxide precipitation to be determined. If hematite precipitation, via sulfide oxidation, genuinely persisted until more recently than supergene enrichment, liberated S and Cu (the latter from chalcopyrite) likely contributed to the oxide zone mineral assemblages observed at both deposits, which include atacamite (Cu-chloride), brochantite (Cu-sulfate) and gypsum (Bouzari & Clark, 2002; Cameron et al. 2007; Reich et al., 2008). Reich et al. (2009) reported Pleistocene ^{230}Th - ^{234}U ages for intergrown gypsum and atacamite from several PCDs, including Spence, showing that S and Cu mobility continued until much more recently than proposed by previous models of weathering and enrichment.

3. Methods

3.1. (U-Th-Sm)/He Hematite Geochronology

During weathering, trace amounts of radioactive U, Th, and Sm are adsorbed from groundwater onto highly reactive surfaces of ferrihydrite (amorphous precursor to hematite and goethite) (Marshall et al., 2014; McBriarty et al., 2018) and incorporated and immobilized during Fe-oxide crystallisation (Das et al., 2011). High rates of radiogenic ^4He ingrowth make these minerals suitable targets for (U-Th-Sm)/He dating (Farley & Flowers, 2012). The closure temperature for He in hematite is dependent on crystallite size (generally ~ 60 to $>100^\circ\text{C}$) (Farley & Flowers, 2012), below which there is near-quantitative He retention at all scales (Bähr et al., 1994; Farley, 2018; Lippolt et al., 1993). Proton irradiation experiments by Farley (2018) showed that a 20 nm hematite crystal within a polycrystalline aggregate will retain $>90\%$ of its ingrown He over 100 Myr at 30°C . Thus, without reheating, ages for low-temperature hematite represent crystallisation, enabling the study of continental weathering histories (Monteiro, Vasconcelos, & Farley, 2018; Monteiro, Vasconcelos, Farley, & Lopes, 2018; Pidgeon et al., 2004; Riffel et al., 2016; Shuster et al., 2012; Vasconcelos et al., 2013) and weathering front propagation (Cooper et al., 2016; Deng et al., 2017; Heim et al., 2006).

3.1.1. Sample Collection, Characterization, and Preparation

At Spence, the hematitic weathered zone varies from 30–100 m thick. Minor hematite also occurs within the subjacent enriched zone, on fracture surfaces and within partially weathered veins which formed high-permeability pathways for descending, weakly oxidising fluids (Lichtner & Biino, 1992). Hema-

Figure 2. (a) Cerro Colorado cross-section modified from Bouzari and Clark (2002). The modern water table lies at the base of the weathered zone in the western part of the deposit but is assumed to slope westward, consistent with the drainage direction of the Quebrada de Parca. (b) View of the Cerro Colorado pit in 1995 (from Bouzari & Clark, 2002), showing cover rocks (ignimbrites and El Diablo Formation gravels) and the supergene anatomy of the deposit. (c) Spence cross-section modified from Cameron and Leybourne (2005). The modern water table approximates the gravel-bedrock contact. (d) View of the North Zone at Spence, showing the Atacama Gravels covering the deposit and the metasedimentary Cerritos Bayos Formation country rocks. The 9.47 ± 0.04 Ma ash layer dated by Sun et al. (2018) lies near the base of the Upper Member of the gravels.

tite-bearing veins and fracture surfaces were sampled from two drill cores in the north zone (SPD1848 and SPD3024, 300 m apart) and one in the south zone (SPD0402) (Figure 1), where the weathered zone is 32 and 48 m thick, respectively. Samples from SPD1848 span the full thickness of the weathered zone, whereas samples from SPD0402 span the lower half of the weathered zone due to the availability of suitable material. Hematite from SPD3024 was taken from the zone of sulfide enrichment, extending the depth range of sampling beneath the ultimate redox front. Hematite was identified in drill core by its dark red to black appearance, textural characteristics (boxwork or botryoidal habit), and red streak. Mineral identification was confirmed via SEM analysis and Raman spectroscopy of polished thin sections. Dated samples were selected from mm to cm scale veins or fracture fills free from contamination and mineral intergrowth.

3.1.2. Analytical Methodology

Samples were extracted from drill core using a micro-saw and crushed to ≤ 1 mm. Seventy-two fragments of hematite (mean fragment weight = 46 μg) were picked manually under a binocular microscope and their mineralogy confirmed by Raman spectroscopy. (U-Th-Sm)/He dating was undertaken at the Caltech Noble Gas Laboratory, following the single aliquot method (Farley, 2002; House et al., 2000). Individual hematite fragments were loaded into Pt tubes and degassed by incremental heating with a Nd-YAG laser. To ensure complete extraction of He, samples were heated to $>1,000^\circ\text{C}$. To avoid parentless He and erroneously high dates due to partial U-loss during hematite-magnetite transformation, He extraction was conducted under high pO_2 (100 torr), buffering the transition to $>1,200^\circ\text{C}$; above the temperature of complete He degassing (Hofmann et al., 2020). Isotope-dilution measurements of ^4He were made with an enriched ^3He spike, using a Pfeiffer Vacuum quadrupole mass spectrometer. U, Th, and Sm were measured on the same aliquots (dissolved in HCl for 12 h at 95°C , then dried and the precipitate re-dissolved in HNO_3) using an Agilent 8800 triple-quadrupole ICP-MS (Hofmann et al., 2017). (U-Th-Sm)/He ages were calculated according to Farley (2002). Since aliquots were taken from structures much larger than the typical alpha-particle stopping distance in hematite of 13–16 μm (Ketcham et al., 2011), no correction for alpha-ejection or -implantation was applied.

3.2. Oxygen Isotope Analysis

The $\delta^{18}\text{O}$ composition of weathering-derived hematite (and goethite) ($\delta^{18}\text{O}_{\text{H(G)}}$) is fixed during crystallisation (Yapp, 2001). Rapid isotopic exchange between water and ferrihydrite promotes equilibrium, and preserved $\delta^{18}\text{O}_{\text{H(G)}}$ signatures reflect the temperature and average fluid composition during mineral formation (Bao & Koch, 1999; Yapp, 1987). Transformation of ferrihydrite likely occurs over days to ~ 100 years (much shorter timescales than the multi-Myr weathering periods which affect PCDs), depending on temperature and pH (Das et al., 2011). Fe-oxides remain closed to later oxygen exchange with groundwater at ambient temperatures (Bao & Koch, 1999). Thus, $\delta^{18}\text{O}_{\text{H(G)}}$ compositions have been used to constrain continental climate change (Yapp, 2001), identify the nature of fluids present during alteration of hypogene base-metal deposits (Cruise et al., 1999), and track latitudinal variation in the isotopic composition of meteoric water during weathering (Miller et al., 2017).

3.2.1. Oxygen Isotope Sample Collection, Characterization, and Preparation

Hematite samples, identified by appearance in hand sample and SEM observations on corresponding thin sections, were selected from three drill holes at Spence and four holes at Cerro Colorado. Samples were crushed/micro-drilled to obtain several milligrams of chips and powder for analysis. Raman spectroscopy was used to confirm the mineralogy of samples JSC17-069 and FC1649. The composition of Fe-oxide extracted from fracture surfaces for two samples from drill hole SPD0551 (JSC17-068 and JSC17-072), and all of the Cerro Colorado samples, for which no thin sections were available, was determined by non-quantitative powder XRD following standard analytical procedures (Bish & Post, 2018). These samples yielded similar spectra, best interpreted as a mixture of hematite and goethite (referred to as hematite/goethite)). At equilibrium, low-temperature (25 – 120°C) hematite and goethite are isotopically indistinguishable (Bao & Koch, 1999; Yapp, 1990), allowing calculation of fluid values using the same mineral-water fractionation equation. The isotopic effect of quartz present in several Cerro Colorado samples was accounted for via aqua regia dissolution and isotopic measurements on quartz separates (see Supporting Information).

3.2.2. Oxygen Isotope ($\delta^{18}\text{O}$) Analysis Via Laser Fluorination

Oxygen isotope analysis of 21 Fe-oxide samples (15 from Spence and six from Cerro Colorado) was conducted at the SUERC Stable Isotope Facility via laser fluorination (Giuliani et al., 2005). For each measurement, 3–5 mg of Fe-oxide was heated with a CO_2 laser in the presence of a fluorine-based reagent (ClF_3). After passing through an in-line Hg-diffusion pump, liberated oxygen was converted to CO_2 using a heated rod of platinized graphite. Isotopic measurements were made using a BG Optima dual-inlet mass spectrometer. Isotopic values were calculated using the mass measurements of CO_2 isotopologues and are reported as $\delta^{18}\text{O}\text{‰}$ relative to Vienna Standard Mean Ocean Water (VSMOW). Calibration on three secondary standards (UWG2, GP147 (international garnet standards) and YP2 (internal quartz standard)) yielded a standard error of 0.07 and $R^2 = 0.9999$. Internal uncertainty on the isotopic measurements is $<0.1\text{‰}$ (1σ).

4. Results

4.1. (U-Th-Sm)/He Geochronology

At our study sites, empirical evidence such as the presence of hematite in former hypogene sulfide veins (originally containing pyrite \pm chalcopyrite and minor quartz) (Figure 3a), boxwork texture (semi-pseudomorphic replacement of cubic pyrite crystals by hematite) (Figure 3b) and microscale textural relationships between spherulitic Fe-oxides and embayed pyrite (Figure 3c) show that hematite has formed through sulfide oxidation, supporting the use of hematite dating to track the paleo-weathering front.

Hematite occurs as amalgamated micro-spheres or polycrystalline aggregates, commonly exhibiting layering on the scale of microns to tens of microns (Figure 3d). It is unclear whether layers are Liesegang bands, formed by geochemical self-organization during precipitation from a supersaturated solution in a single depositional event, or growth layers formed by discrete precipitation events. In the latter case, all ages (new and previously published discussed here) will be averages of the individual growth events contained within each dated fragment (Heim et al., 2006).

Hematite precipitation at Spence records continuous weathering from the middle Miocene to the Pleistocene, with ages tightly clustered in both the North and South Zones (Table 1; Figures 4a–4d). Hematite in North Zone hole SPD1848 formed between 10.5 and 2.2 Ma, although only two fragments yielded ages younger than 5.8 Ma. In South Zone hole SPD0402, most ages fall between 8.6 and 2.7 Ma, although two fragments, situated ~ 50 m beneath the gravel-bedrock contact, yielded older ages of 12.4 and 14.7 Ma. As hematite may continue to precipitate in the weathering zone after initial water table drop (e.g., while residing in the capillary fringe or during transient wetting through water table fluctuation during overall descent), we are most interested in the oldest ages within the clustered data, which mark the onset of generally oxidizing conditions and which we interpret as a record of relative water table descent. Regression through the oldest ages at each sampled depth allows rates of relative water table descent to be estimated; 23.9 ± 19.7 m/Myr in the North Zone and 17.6 ± 9.2 m/Myr in the South Zone (2σ error). If these general trends are extended to the top of the weathered zone, we may expect to find hematite of similar age at the gravel-bedrock contact in both the North and South Zones of the deposit, between ~ 10.2 and ~ 10.8 Ma, although the lack of hematite suitable for dating in the upper part of the weathering profile in SPD0402 (South Zone drill hole) does not allow us to test this hypothesis. Hematite from hole SPD3024, which lies beneath the ultimate redox front, yields ages between 14.0 and 4.8 Ma and a younging-with-depth relationship is not observed.

Continued hematite precipitation until ~ 2 Ma at the ultimate redox front in both the North and South Zones could suggest that the water table rose to its present position after this time. However, it is possible that these young ages instead reflect late uranium addition from groundwater, as has been documented in hematite from the Navajo Sandstone (Reiners et al., 2014). Uranium addition is consistent with the high eU and low Th/U recorded in the youngest aliquots of Spence samples EB16128 and JSC17-186 and Cerro Colorado samples FC1478 and FC1483 (see Supporting Information), although this does not affect our overall interpretation of the data.

Previously published hematite results for Cerro Colorado (Cooper et al., 2016) are shown for comparison in Figures 4e and 4f. Cooper et al. (2016) presented sample ages from different areas on a single age-elevation

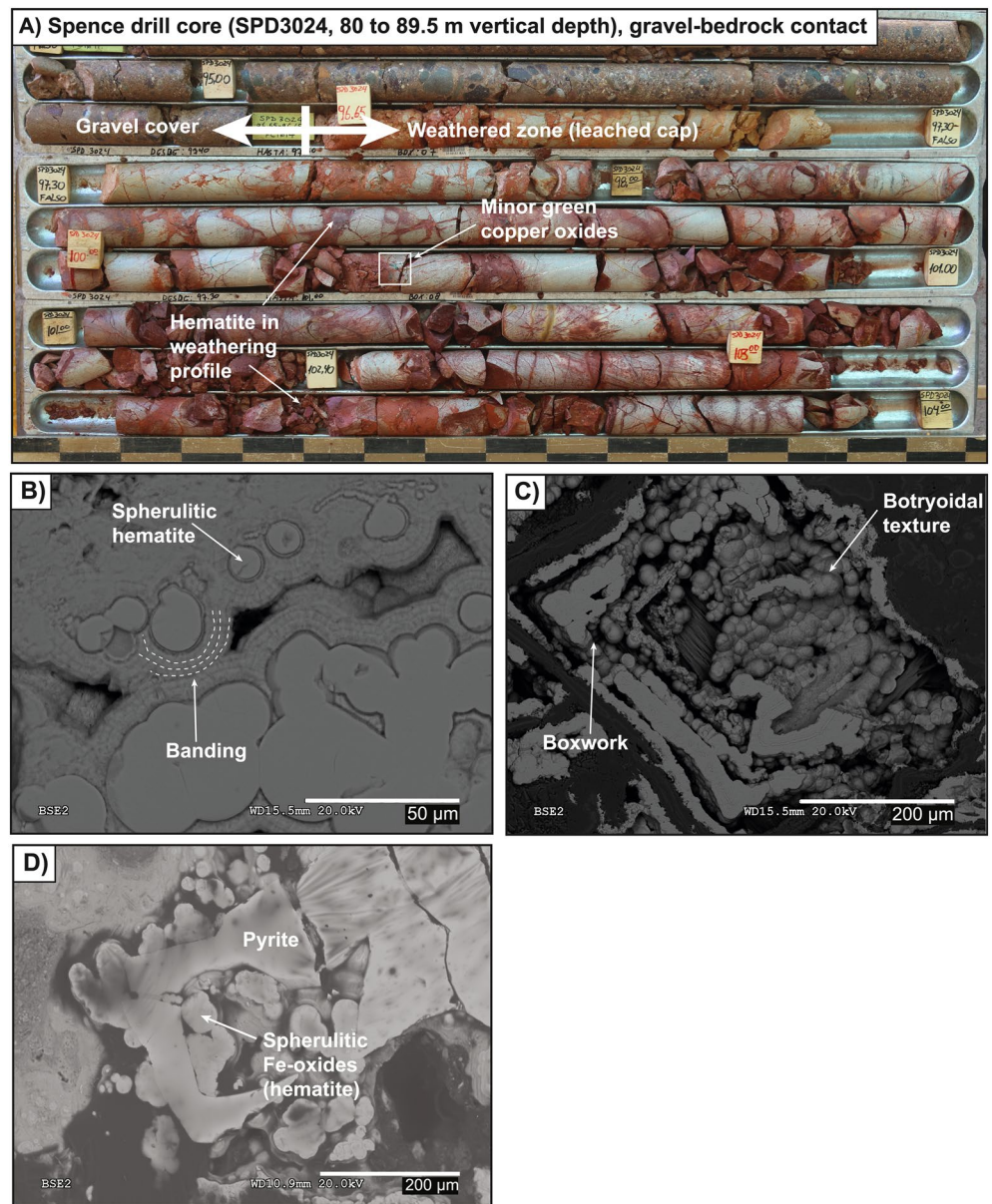


Figure 3. (a) Spence drill-core from hole SPD3024 showing hematite-bearing leached cap rocks beneath gravel cover (wooden markers indicate down-hole depth in meters). In this upper section of the leached cap, weathering is pervasive and all primary sulfides have been replaced by Fe oxides. The host rocks in this core are fine-grained metasediments of the Cerritos Bayos Fm. Minor green oxide mineralization can be seen between 97.30 and 101.00 m. (b–d) Backscattered electron images of representative hematite textures from Spence drill hole SPD0402. (b) Characteristic spherulitic (botryoidal) hematite showing growth banding. (c) Pseudomorphic (boxwork) replacement of a primary sulfide crystal (probably pyrite based on its cubic habit) with botryoidal hematite. (d) An embayed pyrite crystal, collected from the base of the weathering profile, that has been only partially replaced by spherulitic hematite.

plot, assuming a horizontal water table. To account for the westward slope of the land surface and the water table (Section 5.1), we replot these data, normalised to a sloping water table (Figure 4g).

4.2. Iron Oxide Oxygen Isotope Analysis

Fe-oxide samples from Spence yielded $\delta^{18}\text{O}$ values between +5.7‰ and +11.2‰, whereas samples from Cerro Colorado were found to be isotopically lighter (−3.14‰ to +6.76‰) (Table 2). Published

Table 1
Spence (U-Th-Sm)/He Hematite Ages and Compositions

Sample name	Hole ID	Elevation (m a.s.l.)	(U-Th-Sm)/		He age (Ma)	±2σ (Ma)	Weight (μg)	Al		Fe		Al		U		Th		Sm		He		Th/U	eU (ppm)
			He age (Ma)	±2σ (Ma)				Al (μg)	±1σ	Fe (mol-%)	±1σ	Al (mol-%)	±1σ	U (ppm)	±1σ	Th (ppm)	±1σ	Sm (ppm)	±1σ	He (nmol/g)	±1σ		
JSC17-025-h01	SPD0402	1625.5	8.99	0.24	42.84	1.13	0.06	0.00	99.5	0.4	10.25	0.28	0.67	0.04	3.18	0.17	0.51	0.01	0.07	10.41			
JSC17-025-h03	SPD0402	1625.5	8.21	0.22	50.82	1.53	0.07	0.00	99.4	0.4	10.39	0.32	0.28	0.03	3.89	0.25	0.47	0.01	0.03	10.45			
JSC17-025-h04	SPD0402	1625.5	8.56	0.21	50.04	0.99	0.25	0.01	98.5	1.5	11.09	0.23	0.47	0.03	3.83	0.19	0.52	0.02	0.04	11.19			
JSC17-025-h05	SPD0402	1625.5	7.84	0.34	45.61	0.85	0.08	0.00	99.3	0.5	10.98	0.24	0.32	0.07	3.30	0.27	0.47	0.01	0.03	11.05			
JSC17-025-h06	SPD0402	1625.5	6.42	0.32	33.34	0.91	0.28	0.01	97.5	2.4	12.67	0.38	0.55	0.09	3.07	0.30	0.45	0.01	0.04	12.79			
JSC17-030-h01	SPD0402	1621	7.21	0.40	37.28	0.93	0.09	0.00	98.8	0.7	1.54	0.04	0.58	0.04	1.83	0.15	0.07	0.00	0.38	1.67			
JSC17-030-h02	SPD0402	1621	5.84	0.16	86.78	2.96	0.18	0.00	99.2	0.6	1.81	0.06	0.22	0.02	1.87	0.14	0.06	0.00	0.12	1.86			
JSC17-030-h04	SPD0402	1621	7.64	1.20	37.46	0.34	0.05	0.00	99.6	0.4	1.89	0.07	0.28	0.10	1.75	0.14	0.08	0.01	0.15	1.96			
JSC17-030-h05	SPD0402	1621	7.17	0.48	107.98	3.26	0.19	0.00	99.4	0.5	1.62	0.06	0.16	0.03	1.51	0.12	0.06	0.00	0.10	1.65			
JSC17-030-h06	SPD0402	1621	7.35	0.73	92.81	1.65	0.13	0.00	99.5	0.4	1.61	0.05	0.13	0.04	1.49	0.10	0.07	0.00	0.08	1.64			
JSC17-032-h02	SPD0402	1612.1	6.26	0.39	56.00	1.22	1.67	0.04	91.6	8.1	2.28	0.06	0.84	0.04	0.81	0.07	0.08	0.00	0.37	2.48			
JSC17-032-h03	SPD0402	1612.1	6.26	0.21	38.97	0.79	0.89	0.01	93.2	6.3	2.64	0.06	0.71	0.05	1.24	0.10	0.10	0.01	0.27	2.80			
JSC17-032-h05	SPD0402	1612.1	8.05	0.58	74.23	1.49	0.23	0.00	98.5	0.9	2.99	0.08	0.45	0.05	0.27	0.06	0.14	0.03	0.15	3.09			
JSC17-032-h06	SPD0402	1612.1	7.51	0.38	57.70	0.65	0.38	0.01	97.3	1.9	6.93	0.12	2.85	0.08	0.55	0.06	0.31	0.02	0.41	7.59			
JSC17-033-h02	SPD0402	1612	4.93	0.15	73.49	2.69	0.50	0.01	97.3	1.9	6.32	0.24	4.80	0.19	0.76	0.05	0.20	0.00	0.76	7.42			
JSC17-033-h03	SPD0402	1612	4.81	0.20	12.82	0.32	0.18	0.00	95.4	4.1	5.36	0.15	7.05	0.23	5.14	0.31	0.18	0.01	1.31	6.98			
JSC17-033-h04	SPD0402	1612	6.67	0.31	62.21	0.91	0.24	0.00	98.2	1.1	6.21	0.12	5.94	0.13	1.04	0.11	0.28	0.02	0.96	7.58			
JSC17-033-h05	SPD0402	1612	14.75	1.72	11.57	0.15	0.05	0.00	97.7	1.3	9.41	0.35	7.00	0.30	0.84	0.29	0.89	0.06	0.74	11.02			
JSC17-033-h06	SPD0402	1612	8.47	0.56	24.50	0.48	0.08	0.00	98.4	0.9	7.63	0.22	7.08	0.21	0.67	0.15	0.43	0.02	0.93	9.26			
JSC17-034-h01	SPD0402	1609.8	2.90	0.08	17.64	0.30	3.44	0.05	62.7	36.2	9.10	0.18	15.55	0.31	31.18	1.33	0.20	0.01	1.71	12.68			
JSC17-034-h02	SPD0402	1609.8	2.70	0.14	6.83	0.24	0.70	0.02	76.4	23.1	8.80	0.34	18.29	0.78	5.93	0.53	0.19	0.01	2.08	13.01			
JSC17-034-h03	SPD0402	1609.8	4.88	0.16	40.54	1.59	1.62	0.04	89.0	10.5	5.37	0.22	10.50	0.43	5.93	0.38	0.21	0.00	1.96	7.78			
JSC17-034-h05	SPD0402	1609.8	3.18	0.38	9.31	0.10	0.04	0.00	98.2	1.4	6.96	0.29	15.76	0.44	1.32	0.40	0.18	0.04	2.26	10.58			
JSC17-035-h01	SPD0402	1609.6	6.25	0.20	72.73	3.06	0.27	0.01	98.7	1.1	4.06	0.17	2.88	0.13	0.85	0.07	0.16	0.00	0.71	4.72			
JSC17-035-h02	SPD0402	1609.6	6.55	0.17	59.56	1.98	0.76	0.01	96.1	3.6	5.38	0.18	5.72	0.20	2.00	0.14	0.24	0.00	1.06	6.70			
JSC17-035-h03	SPD0402	1609.6	6.54	0.17	48.78	1.75	0.36	0.01	97.5	2.1	5.22	0.19	5.40	0.21	0.94	0.10	0.23	0.01	1.03	6.46			
JSC17-035-h04	SPD0402	1609.6	12.40	0.89	27.93	0.36	0.23	0.00	97.3	2.4	6.62	0.16	6.39	0.17	1.61	0.14	0.55	0.03	0.97	8.09			
JSC17-035-h05	SPD0402	1609.6	7.21	0.44	21.34	0.30	0.28	0.00	96.0	3.8	9.31	0.21	9.70	0.30	5.69	0.32	0.45	0.02	1.04	11.54			
JSC17-038-h02	SPD0402	1603.3	4.69	0.23	25.76	0.94	0.05	0.00	99.4	0.5	2.42	0.10	6.52	0.25	0.75	0.09	0.10	0.00	2.69	3.92			
JSC17-038-h04	SPD0402	1603.3	3.56	0.62	17.81	0.32	0.20	0.00	96.7	3.3	2.33	0.16	6.30	0.25	0.80	0.22	0.07	0.01	2.71	3.77			
JSC17-038-h05	SPD0402	1603.3	4.28	0.48	25.22	0.51	0.10	0.00	98.8	1.2	2.47	0.12	7.16	0.21	0.76	0.14	0.10	0.01	2.89	4.12			
JSC17-038-h06	SPD0402	1603.3	5.99	0.50	33.19	1.22	0.14	0.00	98.7	1.3	3.38	0.17	9.56	0.39	1.31	0.17	0.18	0.01	2.83	5.58			
JSC17-039-h01	SPD0402	1603	4.72	0.19	66.23	2.20	0.29	0.01	98.6	1.3	2.79	0.10	4.70	0.16	1.12	0.11	0.10	0.00	1.68	3.87			

Table 1
Continued

Sample name	Hole ID	Elevation (m a.s.l.)	(U-Th- Sm)/ He age (Ma)	±2σ (Ma)	Weight (μg)	Al (μg)	Fe (mol- %)	Al (mol- %)	U (ppm)	±1σ	Th (ppm)	±1σ	Sm (ppm)	±1σ	He (nmol/g)	±1σ	Th/U	eU (ppm)
JSCI17-039-h02	SPD0402	1,603	5.79	0.14	48.79	1.73	0.18	1.1	2.59	0.09	3.74	0.14	1.40	0.10	0.11	0.00	1.44	3.45
JSCI17-039-h05	SPD0402	1,603	5.78	0.24	36.54	1.39	0.29	2.3	2.11	0.08	2.23	0.10	0.85	0.06	0.08	0.00	1.05	2.63
JSCI17-039-h08	SPD0402	1,603	7.88	0.78	39.12	1.28	0.13	1.0	2.48	0.11	3.33	0.14	0.97	0.17	0.14	0.01	1.34	3.25
JSCI17-039-h09	SPD0402	1,603	4.18	0.85	9.21	0.18	0.30	0.1	4.91	0.30	6.00	0.42	2.31	0.40	0.14	0.02	1.22	6.28
JSCI17-179-h01	SPD3024	1591.7	10.0	0.264	99.41	2.09	0.24	0.1	16.50	0.36	0.42	0.02	1.93	0.13	0.90	0.02	16.61	16.60
JSCI17-179-h02	SPD3024	1591.7	9.9	0.248	80.87	1.99	0.18	0.1	11.59	0.29	0.45	0.02	0.13	0.02	0.63	0.01	11.69	11.69
JSCI17-179-h03	SPD3024	1591.7	7.8	0.234	39.70	1.25	0.18	0.1	20.02	0.65	0.45	0.05	0.26	0.03	0.85	0.01	20.12	20.12
JSCI17-179-h04	SPD3024	1591.7	9.1	0.372	92.70	1.58	0.18	0.0	17.24	0.34	0.15	0.03	0.09	0.03	0.85	0.02	17.28	17.28
JSCI17-179-h05	SPD3024	1591.7	6.6	0.26	69.08	1.51	0.14	0.0	18.34	0.44	0.39	0.05	0.18	0.06	0.66	0.02	18.43	18.43
JSCI17-184-h01	SPD3024	1542.3	11.2	0.448	136.40	5.40	0.08	0.1	7.69	0.31	0.08	0.01	0.24	0.02	0.47	0.01	7.71	7.70
JSCI17-184-h02	SPD3024	1542.3	10.2	0.348	87.89	3.92	0.20	0.1	8.49	0.39	0.38	0.03	0.38	0.03	0.47	0.01	8.58	8.58
JSCI17-184-h03	SPD3024	1542.3	14.0	0.536	30.91	1.18	0.05	0.0	11.69	0.46	0.35	0.05	0.55	0.05	0.89	0.02	11.77	11.77
JSCI17-184-h04	SPD3024	1542.3	8.8	0.28	108.67	3.46	0.15	0.0	9.97	0.33	0.16	0.03	0.32	0.05	0.48	0.01	10.01	10.01
JSCI17-184-h05	SPD3024	1542.3	11.2	0.33	57.48	1.16	0.06	0.0	9.64	0.21	0.32	0.06	0.31	0.06	0.59	0.01	9.72	9.72
JSCI17-186-h01	SPD3024	1530.7	9.2	0.25	148.17	3.89	0.25	0.1	4.37	0.12	2.94	0.08	0.39	0.03	0.25	0.00	5.06	5.04
JSCI17-186-h02	SPD3024	1530.7	4.8	0.092	39.80	0.75	0.66	0.1	24.59	0.49	35.58	0.73	10.98	0.50	0.86	0.03	33.01	32.78
JSCI17-186-h03	SPD3024	1530.7	8.7	0.254	130.35	3.56	0.30	0.0	7.83	0.22	3.92	0.11	0.34	0.04	0.42	0.01	8.75	8.73
JSCI17-186-h04	SPD3024	1530.7	8.4	0.356	84.48	3.52	0.13	0.0	3.70	0.16	2.62	0.12	0.27	0.05	0.20	0.01	4.31	4.30
JSCI17-186-h05	SPD3024	1530.7	11.6	0.634	62.38	1.16	0.15	0.0	3.51	0.10	9.02	0.20	1.04	0.10	0.36	0.01	5.63	5.58
EB16118h1	SPD1848	1671.2	8.70	0.85	17.59		0.04		6.50	0.25	18.69	0.68	3.04		0.52	0.00	2.88	10.80
EB16118h2	SPD1848	1671.2	6.80	1.01	6.50		0.04		7.82	0.38	33.32	1.72	3.91		0.58	0.00	4.26	15.48
EB16119h1	SPD1848	1666.3	8.01	0.74	12.42		0.03		9.56	0.36	13.23	0.66	7.27		0.55	0.00	1.38	12.61
EB16119h2	SPD1848	1666.3	8.64	0.60	35.03		0.03		7.46	0.22	6.25	0.24	0.99		0.42	0.00	0.84	8.90
EB16119h3	SPD1848	1666.3	6.99	0.64	18.43		0.04		11.78	0.41	12.25	0.61	3.89		0.56	0.00	1.04	14.60
EB16120h1	SPD1848	1665.1	6.88	0.39	56.31		0.06		8.49	0.17	1.30	0.08	1.19		0.33	0.01	0.15	8.79
EB16120h2	SPD1848	1665.1	8.63	0.61	27.10		0.04		11.17	0.32	2.82	0.24	2.08		0.56	0.00	0.25	11.81
EB16120h3	SPD1848	1665.1	10.48	0.60	40.85		0.03		9.40	0.19	1.42	0.09	1.22		0.55	0.01	0.15	9.72
EB16122h1	SPD1848	1661.7	7.40	0.55	62.24		0.05		4.13	0.13	2.97	0.14	0.58		0.19	0.00	0.72	4.81
EB16122h2	SPD1848	1661.7	8.56	0.65	88.35		0.04		1.54	0.05	4.69	0.12	0.36		0.12	0.00	3.04	2.62
EB16123h1	SPD1848	1659.1	2.34	0.11	53.31		0.04		19.77	0.27	7.16	0.18	0.57		0.27	0.00	0.36	21.42
EB16123h3	SPD1848	1659.1	5.78	0.40	32.36		0.03		22.98	0.64	12.78	0.58	10.18		0.82	0.00	0.56	25.92
EB16125h1	SPD1848	1656.2	8.98	0.45	111.19		0.05		5.39	0.08	5.82	0.11	0.84		0.33	0.02	1.08	6.73
EB16125h2	SPD1848	1656.2	10.05	0.50	78.48		0.08		6.19	0.10	5.76	0.12	0.78		0.41	0.02	0.93	7.51

Table 1 Continued	Sample name	Hole ID	Elevation (m a.s.l.)	(U-Th- Sm)/ He age (Ma)	$\pm 2\sigma$ (Ma)	Weight (μg)	Al (μg)	$\pm 1\sigma$	Fe (mol- %)	Al (mol- %)	U (ppm)	$\pm 1\sigma$	Th (ppm)	$\pm 1\sigma$	Sm (ppm)	$\pm 1\sigma$	He (nmol/g)	Th/U	eU (ppm)
	EB16125h3	SPD1848	1656.2	10.17	0.55	68.26	0.03				6.18	0.12	4.95	0.12	0.72	0.01	0.41	0.80	7.32
	EB16126h1	SPD1848	1650.1	8.07	0.63	79.62	0.05				4.89	0.15	3.22	0.17	0.53	0.00	0.25	0.66	5.63
	EB16126h2	SPD1848	1650.1	9.67	0.65	107.16	0.06				3.49	0.10	2.30	0.09	0.41	0.00	0.21	0.66	4.02
	EB16126h3	SPD1848	1650.1	9.74	0.59	68.07	0.03				3.78	0.09	2.45	0.08	0.41	0.01	0.23	0.65	4.35
	EB16128h1	SPD1848	1,642	9.50	0.67	19.61	0.04				9.39	0.28	9.15	0.33	13.67	0.00	0.60	0.97	11.50
	EB16128h2	SPD1848	1,642	2.33	0.16	72.13	0.04				18.65	0.47	9.98	0.38	0.86	0.00	0.27	0.53	20.95
	EB16128h3	SPD1848	1,642	2.20	0.15	24.07	0.04				35.39	0.76	13.92	0.50	1.53	0.00	0.46	0.39	38.59

hematite(goethite)-water fractionation factors at 25°C range from -8.96‰ (Zheng & Simon, 1991; based on thermodynamic calculations) to 6.04‰ (Yapp, 1990; based on synthesis experiments), which is important because the isotopic composition of the parental water is the predominant control on that of the precipitate (Miller et al., 2017; Sultan, 2015; Yapp, 1987). We apply the fractionation factor of Yapp (1990) as it is representative of samples from natural environments (Miller et al., 2017; Yapp, 2000), and yields calculated fluid compositions within previously published ranges for meteoric and groundwater documented near Cerro Colorado (Aravena et al., 1999; Fritz et al., 1981) and Spence (Cameron & Lebourne, 2005). We assume a temperature of 25°C when calculating parental fluid isotopic compositions based on groundwater temperatures of 20–29°C (BHP data) measured in drill holes around Spence and elsewhere in the Central Depression and Precordillera close to Cerro Colorado (Fritz et al., 1981; see Supporting Information).

5. Discussion: Geochronological and Geochemical Constraints on Weathering at Cerro Colorado and Spence

5.1. Landscape Evolution, Canyon Incision, and Water Table Movement at Cerro Colorado

The north side of Cerro Colorado is cut by the Quebrada de Parca, one of several endorheic drainages linking the Andean Precordillera with regional base level in the Central Depression (Figures 1b, 1c, and 2d). Cooper et al.'s (2016) hematite (U-Th-Sm)/He data appear to support a prolonged period of water table stability between ~ 31 and ~ 16 Ma, with water table descent < 16 Ma linked to aridity-induced incision of the Quebrada de Parca. However, we suggest that at least some of the age-elevation trend observed by Cooper et al. (2016) is an artifact of sample locations and the slope of the water table, and present a reinterpretation of these data constrained by published paleo-climate and sedimentological records, and geomorphological relationships observed in satellite imagery, which imply later incision at ~ 11 Ma.

Outcropping both north and south of the Quebrada de Parca are Miocene El Diablo Formation (EDF) gravels (Blanco et al., 2012), deposited by a large distributive fluvial system (García et al., 2011; Jordan et al., 2010, 2014). K-Ar ages of volcanic units within the uppermost EDF sediments, including samples located ~ 5 km downslope of Cerro Colorado, suggest that deposition ended between ~ 11.9 and ~ 11.2 Ma (Blanco et al., 2012; Fariás et al., 2005; García et al., 2004, 2011), forming a regional aggradational paleo-surface (Evenstar et al., 2017, 2020). The Quebrada de Parca dissects a weakly developed drainage network on this surface, showing that canyon incision must post-date EDF deposition. This supports the view that the onset of modern hyperaridity, which created the conditions for both surface abandonment and canyon incision, occurred between ~ 12 and 10 Ma, in agreement with the onset of canyon incision elsewhere in the Precordillera at ~ 10 Ma (e.g., García et al., 2011; Hoke et al., 2007; Schlunegger et al., 2006).

Proximal to Cerro Colorado, the surface of the EDF slopes westward $2.7\text{--}3.7^\circ$. Between the Precordillera and the Central Depression, the Quebrada de Parca drops from $\sim 4,000$ to $\sim 1,000$ m a.s.l., and recent geophysical (TDEM) data from the lower reaches of the Precordillera near to Cerro Colorado show the water table approximates a subdued version of the surface topography (Viguiet et al., 2018). Based on geomorphic analysis of the channel profile, Cooper et al. (2016) showed that canyon incision was driven by climatic factors and that post-incision tilting of this section of the Precordillera has been negligible since the middle Miocene. Therefore, we assume the modern surface and water table slopes are representative of those during development of the preserved weathering profile at Cerro Colorado. To account for the lateral separation of sampled drill holes (1.5 km in the direction of slope), we replotted the (U-Th-Sm)/He data in terms of elevation relative to a water table with a westward slope of 2.7° (Figure 4g). By normalizing the data in this way, the previously apparent break in slope at ca. 16 Ma is no longer obvious.

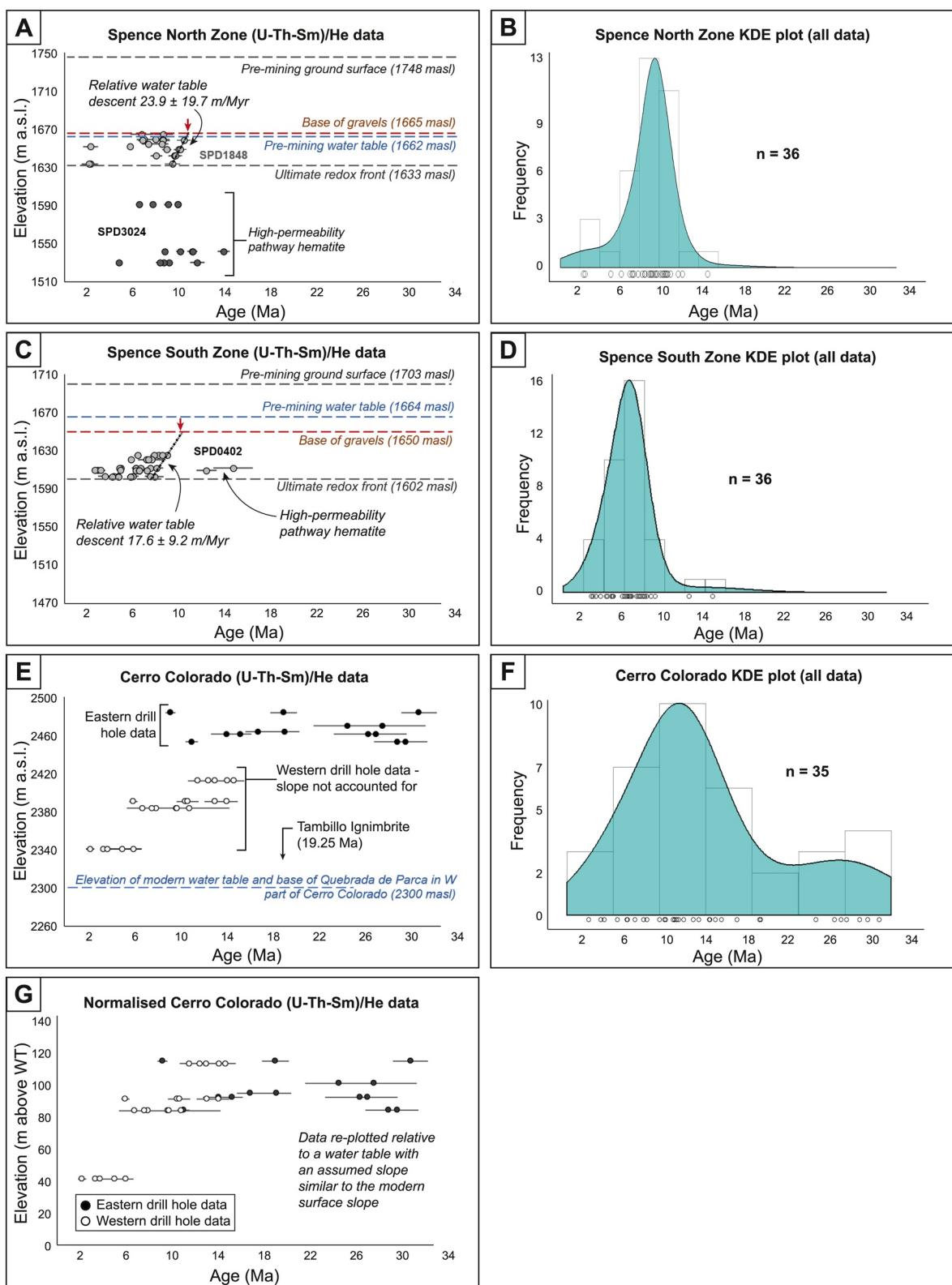


Figure 4.

We suggest that following the end of exhumation-driven relative water table descent, possibly by ~ 30 Ma (which marks the beginning of prolonged hematite precipitation), and certainly by 19.25 Ma (minimum age constrained by the Tambillo ignimbrite; Bouzari & Clark, 2002), the water table at Cerro Colorado remained relatively stable, until a reduction in MAR, from ~ 130 to < 20 mm, between 12 and 11 Ma (Jordan et al., 2014) ended deposition of EDF sediments and drove incision of the Quebrada de Parca and associated water table decay (Figure 5a). Our reassessment implies 300 m incision (the depth of the Quebrada de Parca proximal to Cerro Colorado) within ~ 11 Myr; an overall incision rate of ~ 27 m/Myr, in agreement with estimates for other canyons in the Precordillera (Evenstar et al., 2020). However, the overall impact of incision on the elevation of the water table is of lower magnitude (~ 85 m) as the water table was already situated at a depth of ~ 150 – 200 m when incision began (Figure 5a).

5.2. Landscape Evolution and Water Table Movement at Spence

Most hematite ages above the ultimate redox front at Spence are younger than ~ 10.5 Ma (Figure 4). The cluster of hematite ages starting at this time across a range of depths likely reflects pervasive weathering following relative water table descent. We attribute two older ages from beneath the ultimate redox front in the North Zone (14.7 and 12.4 Ma; Figure 4a) to incipient oxidation along high-permeability pathways, such as faults and fractures, which allowed oxygenated water to penetrate beneath the paleo-water table (Lichtner & Biino, 1992). Similarly, two middle Miocene-aged samples from the South Zone (Figure 4c) are interpreted as hematite that formed along high-permeability pathways prior to water table descent.

In the absence of canyon incision, we suggest that weathering front propagation at Spence was controlled by exhumation-driven relative water table descent. The position of the ultimate redox front was attained when exhumation ceased, and the estimated rates of relative water table descent (23.9 ± 19.7 m/Myr in the north and 17.6 ± 9.2 m/Myr in the south) approximate rates of exhumation prior to cover deposition. The apparent end of exhumation in the North Zone, constrained by a 9.50 ± 0.67 Ma (2σ) hematite at the ultimate redox front (Figure 4a), coincides with the age of a 9.47 ± 0.04 Ma ash layer within the overlying gravels (Figure 5b; Sun et al., 2018). Assuming steady-state erosion and water table descent, the switch from erosion to local cover deposition occurred in the late Miocene (Figure 5b), at least 10 Myr after Cerro Colorado and coeval with the onset of hyperaridity. Our observations at Spence bear some similarity to the thin cover of Arriero Gravels overlain by a 9.52 Ma tuff layer at the Mirador mine in the Centinela District, described by Riquelme et al. (2018), although the supergene enrichment at Spence (~ 44 – 20 Ma; Rowland & Clark, 2001) occurred earlier than in the Centinela District (~ 25.2 – 12.6 Ma; Riquelme et al., 2018).

At Spence, the modern water table depth (86 m in the North Zone and 39 m in the South Zone) is not significantly different to the depth of the ultimate redox front below the erosional paleo-surface/base of the gravel cover (32 m in the North Zone and 48 m in the South Zone). Although increasing aridity was probably important in the switch from erosion to deposition (first of sheet flood sediments, followed by drier debris flows; Riquelme et al., 2007; Sun et al., 2018), and then to surface abandonment, prolonged hyperaridity has had little effect on the position of the water table, which did not get progressively deeper from the late Miocene onward (Figures 4a, 4c, and 5b). Similarly, the depth of the modern water table in the Central Depression west of Cerro Colorado is ~ 50 m in some areas (Viguier et al., 2018). Although it is unclear when the water table at Spence attained its present position near the gravel-bed-rock contact, this likely occurred during the Pliocene, based on the youngest clustered ages observed in both the North and South Zones.

Figure 4. Spence and Cerro Colorado (U-Th-Sm)/He hematite data. (a–d) At Spence, most of the preserved hematite formed from the late Miocene (~ 10.5 Ma) onward. (a and c) Age-elevation plots show that the modern water table, which approximates the position of the gravel-bedrock contact, is elevated relative to the ultimate redox front. Rates of relative water table descent are similar in the North and South zones. Red arrows indicate the intercept of each trendline with the gravel-bedrock contact, showing the expected onset of weathering in the uppermost part of the preserved profile assuming steady state water table descent. (b and d) Kernel Density Estimator (KDE) plots show the distribution of ages from each of the zones, clustered between the late Miocene and Pliocene. (e and f) Age-elevation and KDE plots of Cerro Colorado data from Cooper et al. (2016) distributed between ~ 31 and ~ 2 Ma. G: Cerro Colorado data replotted as elevation above a water table with an assumed westward slope of 2.7° (the minimum slope for the El Diablo Formation surface).

Table 2

Hematite (Goethite) Oxygen Isotope Results and Corrected Fluid Values (Using the Fractionation Factor of Yapp [1990]; $1,000\ln\alpha = 1.63 \times (10^6/T^2) - 12.3$), Where $1,000\ln\alpha$ Refers to the Fractionation Factor and T is Temperature in Kelvin

Sample name	Mineralogy	Hole ID/location	Elevation (m a.s.l)	Raw $\delta^{18}\text{O}$ (‰)	$\delta^{18}\text{O}$ (‰)	Fluid $\delta^{18}\text{O}$ (‰)*
JSC17-025	Hematite	SPD0402 (Spence south)	1,625	−17.11	8.62	2.58
JSC17-032	Hematite	SPD0402 (Spence south)	1,612	−15.19	10.77	4.73
JSC17-032	Hematite	SPD0402 (Spence south)	1,612	−14.84	10.89	4.85
JSC17-033	Hematite	SPD0402 (Spence south)	1,612	−15.05	10.91	4.87
JSC17-035	Hematite	SPD0402 (Spence south)	1,609	−15.16	10.79	4.75
JSC17-038	Hematite	SPD0402 (Spence south)	1,603	−15.33	10.63	4.59
JSC17-038	Hematite	SPD0402 (Spence south)	1,603	−14.56	11.17	5.13
JSC17-039	Hematite	SPD0402 (Spence south)	1,603	−17.99	7.56	1.52
LiC17-013	Hematite	SPD0402 (Spence south)	1,603	−15.66	10.31	4.27
LiC17-013	Hematite	SPD0402 (Spence south)	1,603	−15.33	10.39	4.35
JSC17-068	Hem/Goe	SPD0551 (Spence south)	1,620	−16.98	8.63	2.59
JSC17-069	Hematite	SPD0551 (Spence south)	1,620	−17.49	8.08	2.04
JSC17-070	Hematite	SPD0551 (Spence south)	1,620	−17.97	7.58	1.54
JSC17-072	Hem/Goe	SPD0551 (Spence south)	1,612	−15.97	9.69	3.65
JSC17-184	Hematite	SPD3024 (Spence north)	1,542	−19.79	5.67	−0.37
FC1649	Hematite	DDH-05-21 (Cerro Colorado)	2,500	−24.31	0.90	−5.14
FC1644	Hem/Goe	D-DDH-05-21 (Cerro Colorado)	~2,500	−	1.54	−4.50
FC1653	Hem/Goe	D-DDH-099-13 (Cerro Colorado)	~2,500	−	−3.14	−9.18
FC1654	Hem/Goe	D-DDH-099-13 (Cerro Colorado)	~2,500	−	6.76	0.72
FC1675	Hem/Goe	DDH-14-041 (Cerro Colorado)	~2,500	−	1.58	−4.46
FC1697	Hem/Goe	D-DDH-11-076 (Cerro Colorado)	~2,500	−	−3.00	−9.04

Note. The “*” refers to calculated using the fractionation factor of Yapp (1990).

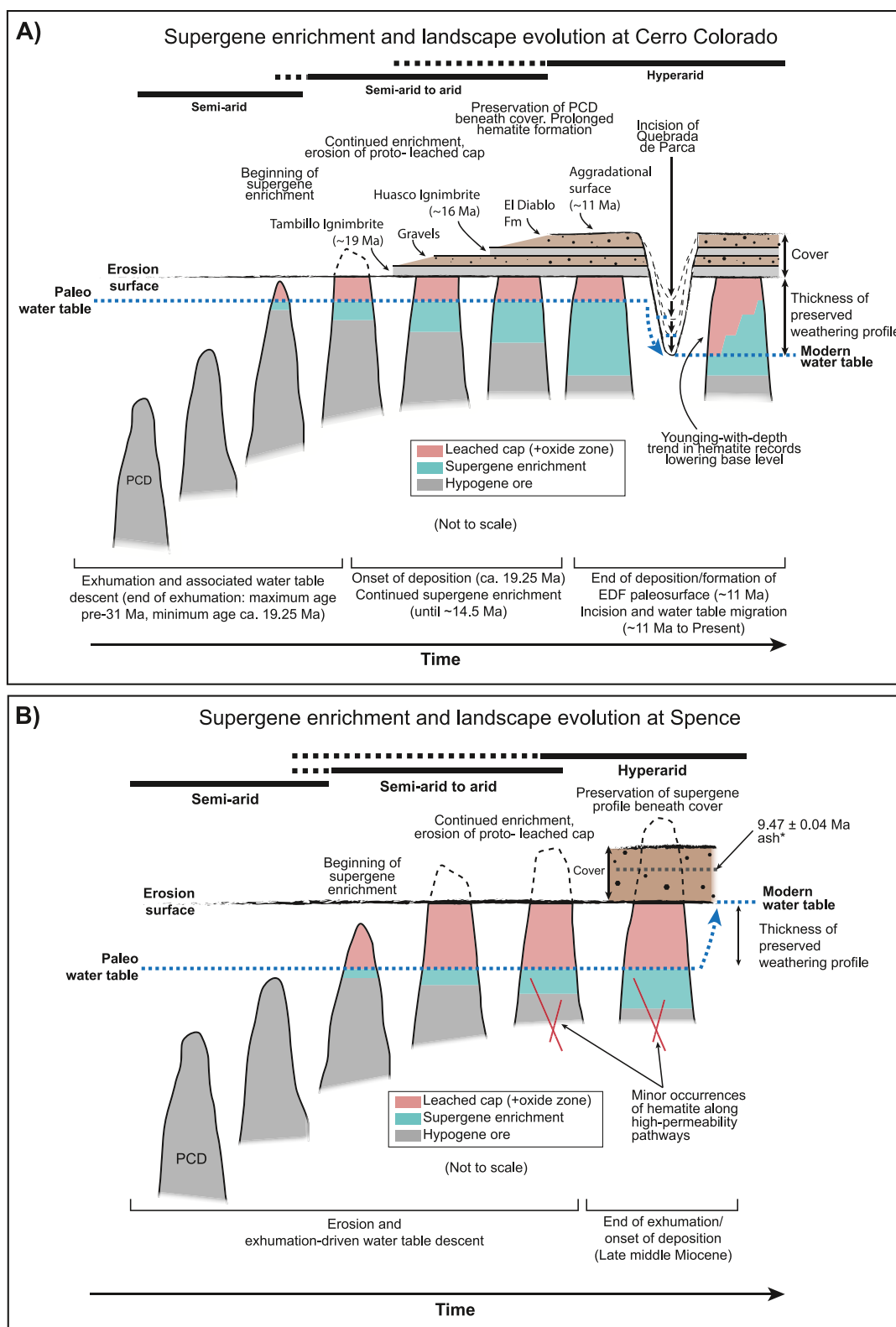
5.3. The Relative Importance of Climate and Tectonics on Water Table Descent and Supergene Enrichment

As climate desiccation in the Atacama occurred on a regional scale, subjecting many PCDs to comparable environmental conditions, variations in water table depth, supergene enrichment, and weathering zone thickness between different deposits (5–50 m at Spence, 50–200 m at Cerro Colorado, 10–500 m at La Escondida) cannot be explained by spatially variable precipitation. Instead, this variation suggests differences in exhumation histories (Bissig & Riquelme, 2009), local lithological and tectonic controls on aquifer architecture (Jordan et al., 2014), medium to long-range groundwater recharge characteristics (Houston, 2002; Magaritz et al., 1990; Scheihsing et al., 2017) and canyon incision may be important factors.

5.4. Oxygen Isotopes, Groundwater Sources, and the Susceptibility of Water Tables to Post-Hyperaridity Descent

$\delta^{18}\text{O}_{\text{H(G)}}$ compositions have been shown to rapidly equilibrate with, and record, those of weathering fluids, according to the fractionation factor of Yapp (1990) (Miller et al., 2017; Yapp, 1990, 2000). Thus, our calculated groundwater isotopic values demonstrate the relative importance of meteoric versus formation water during PCD weathering and offer clues as to the relative susceptibility of different locations to water table decay in response to increased aridity.

Calculated fluid compositions for Cerro Colorado Fe-oxides ($\delta^{18}\text{O} = (-3.14\text{‰ to }+6.76\text{‰})$) largely overlap the range of measured values for precipitation falling within the Quebrada de Parca catchment at or above the modern elevation of the deposit (Aravena et al. [1999] and Fritz et al. [1981] data; Figure 6). A meteoric



signature is indicative of direct recharge (pre-hyperaridity) or short to medium-range (catchment-scale) indirect recharge (post-hyperaridity), recording groundwater flow through the shallow subsurface according to the Andean basin fill recharge model (Houston 2002; Figure 7). Prior to climate desiccation, groundwater at Cerro Colorado would have been replenished by more rainfall in the upper reaches of the Precordillera infiltrating down to the water table (Jordan et al., 2014; Rech et al., 2019), but the deposit has since been susceptible to water table decay due to decreased meteoric recharge in the Quebrada de Parca catchment, and aridity-induced canyon incision.

At Spence, isotopically light meteoric water, derived from precipitation between 2,500 and 3,000 m a.s.l., has been documented in the eastern area of the deposit, upslope of the ACL, whereas isotopically heavy, saline water has been documented west of the ACL (Figure 6c; Cameron & Leybourne, 2005). Our calculated fluid isotopic values for Spence hematite(goethite) ($\delta^{18}\text{O} = -0.37\text{‰}$ to $+5.13\text{‰}$), from both sides of the ACL (Figure 6c) are much heavier than for Cerro Colorado (Table 2; Figure 6b). Although the elevation-dependent trend of precipitation compositions in Figure 6b could be extrapolated to intercept the range of calculated parent fluid values for Spence hematite, most hematite at Spence formed after climate desiccation and beneath cover, making local precipitation an unlikely water source during weathering. Isotopically distinct groundwaters at Spence (Cameron & Leybourne, 2005) show that meteoric water that arrives via indirect recharge retains its light isotopic signature under hyperarid conditions. Therefore, isotopically heavy groundwater cannot be explained by evaporation or reactive flow of meteoric water through the shallow subsurface. Isotopically heavy groundwater is likely deep formation water, upwelling along weaknesses associated with the ACL (Cameron & Leybourne, 2005). We suggest that the maintenance of a shallow water table at Spence is due to long-range groundwater recharge of basal aquifers in the Pampa del Tamarugal, over long timescales (10^4 – 10^5 years; Jayne et al., 2016), by more consistent precipitation in the high Andes (>100 mm/year MAR above 4,000 m a.s.l.; Jordan et al., 2014). The heavy isotopic signature of hematite-forming water at Spence may be the result of prolonged reactive transport and mixing with hydrothermally circulating waters within the basement (Magaritz et al., 1990) prior to upwelling along the ACL in line with the Toth (1963) model of groundwater flow (Figure 7).

The destructive nature of both techniques precluded obtaining isotopic data for the same hematite fragments that were dated. However, in many cases both measurements were made on hematite from the same veins/fractures and we therefore assume that our isotopic results reflect the composition of groundwater during weathering from the late Miocene onward. The isotopic composition of hematite-forming water at Spence shows deep formation water has contributed to recharge for ≥ 10 Myr, suggesting that the groundwater regime proposed by Cameron & Leybourne (2005) has been long-lived. We propose that the water table at Spence has remained shallow, despite climate desiccation, because of deep recharge fed by consistently higher MAR in the high Andes.

6. Conclusions

We use hematite (U-Th-Sm)/He geochronology and oxygen isotope analysis to compare the timing of weathering and sources of groundwater at two Andean PCDs in different morphotectonic settings—Cerro Colorado, within the Precordillera, and Spence, within the Central Depression. By combining our data with field observations and published sedimentological and geochronological constraints, we draw the following conclusions:

1. At Cerro Colorado, the dissection of an older drainage network on the surface of the El Diablo Formation, combined with published sedimentological and geochronological evidence (dated ash layers within the El Diablo Formation local to the deposit), suggest that incision of the Quebrada de Parca began at ~ 11 Ma (rather than ~ 16 Ma as previously suggested), implying 300 m of incision since the

Figure 5. Models for water table movement and supergene enrichment at Cerro Colorado and Spence. (a) At Cerro Colorado, exhumation-driven water table descent was likely important before ~ 31 Ma, after which the water table remained stable for a prolonged period. At ~ 11 Ma, canyon incision initiated, resulting in a deep modern water table. (b) At Spence, preserved hematite formed later than at Cerro Colorado and the oldest dated cover is a 9.47 Ma ignimbrite (Sun et al., 2018). Exhumation-driven water table descent was important until the late Miocene. The modern water table is elevated relative to the ultimate redox front, approximating the gravel-bedrock contact.

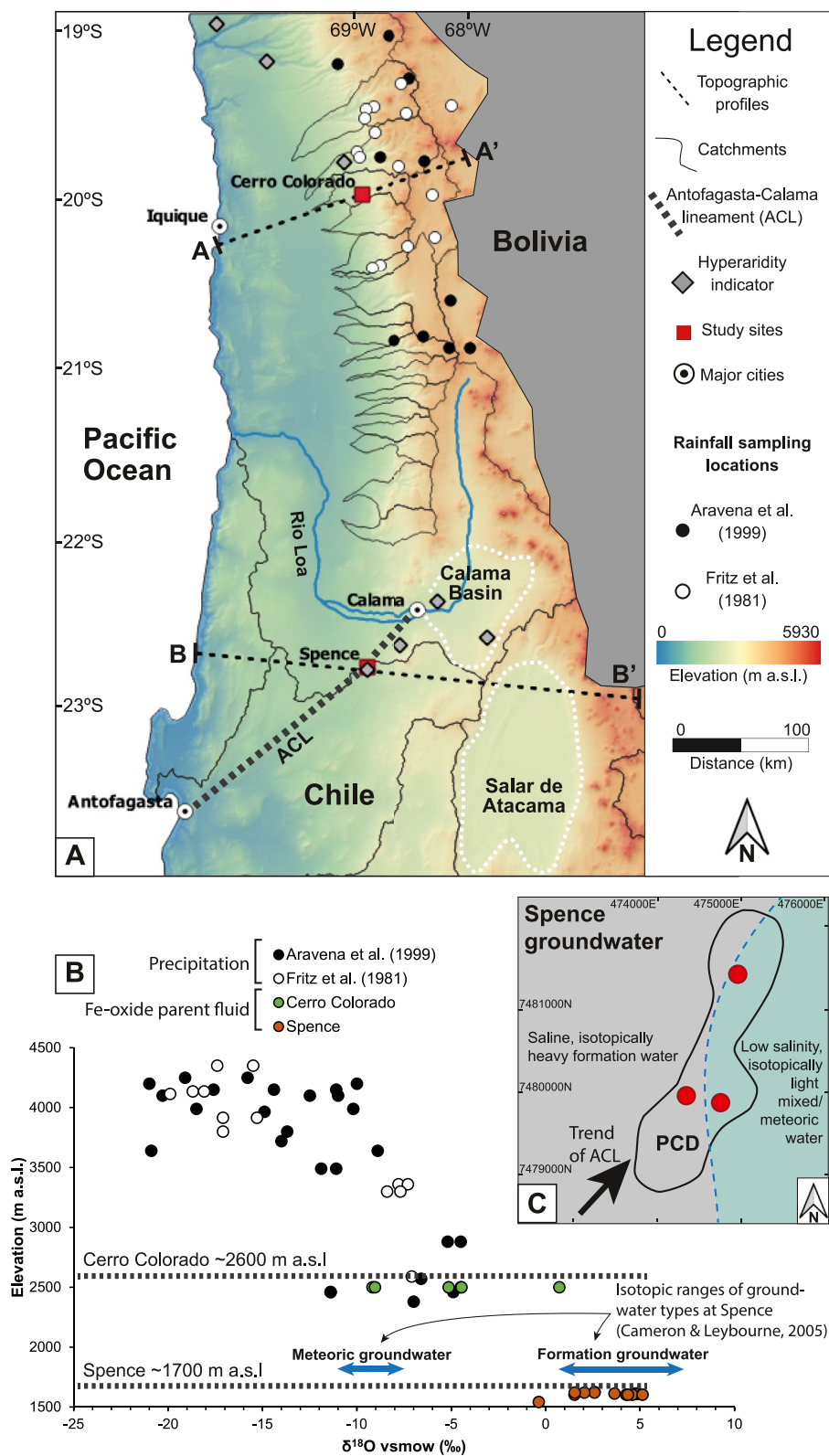


Figure 6.

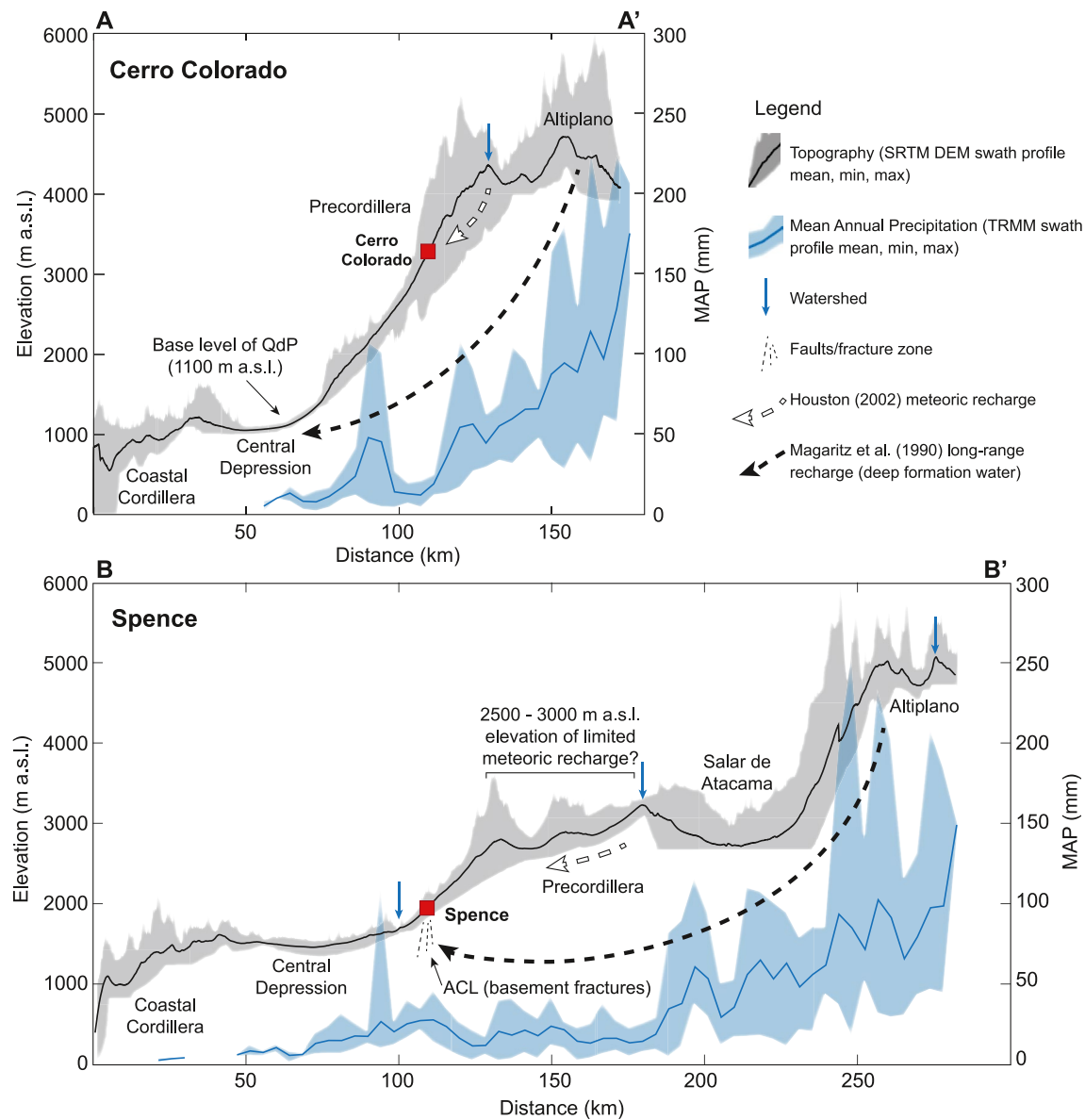


Figure 7. Topographic (SRTM DEM data) and precipitation (TRMM rainfall data; Bookhagen & Strecker, 2012) swath profiles for Cerro Colorado and Spence (accounting for data 20 km either side of lines A-A' and B-B' in Figure 6a). Arrows schematically show indirect recharge pathways. The Houston (2002) basin fill recharge model accounts for water table decay at Cerro Colorado in response to increased aridity and incision of the Quebrada de Parca. At Spence, the water table has remained shallow as the ACL has provided a pathway for upwelling formation water, originating as precipitation in the high Andes and moving through the basement according to the recharge and hydrothermal mixing model of Magaritz et al. (1990).

late Miocene. River base level in the Quebrada de Parca continues to control the position of the modern water table today.

2. Published ages constraining cover deposition suggest exhumation-driven water table descent ceased between ~31 and 19.25 Ma at Cerro Colorado and by 9.47 Ma at Spence, a difference of at least 10 million years. At Spence, the younging-with-depth relationship in the (U-Th-Sm)/He data above the ultimate

Figure 6. (a) Elevation map of northern Chile showing river catchment boundaries along the Precordillera and rainfall sampling locations from Aravena et al. (1999) and Fritz et al. (1981). Locations of isotopic and sedimentological hyperaridity indicators are from Hartley and May (1998) and Rech et al. (2010, 2019) (Section 2.2). Lines A-A' and B-B' are centerlines of the topographic and precipitation swath profiles in Figure 7. (b) Elevation-dependent isotopic composition of rainfall in the Atacama Desert based on data from sampling stations in A, with corrected fluid isotopic values for hematite from Cerro Colorado and Spence. (c) Distribution of groundwater types at Spence (after Cameron & Leybourne, 2005). Red circles show the locations of drill holes sampled at Spence for oxygen isotope analysis in this study.

redox front suggests that exhumation-related water table descent, at a rate of ~ 20 m/Myr, was active prior to gravel deposition. The similarity in age of a ~ 9.47 Ma ash layer within the overlying gravels to a ~ 9.50 Ma hematite fragment precipitated at the ultimate redox front suggests an abrupt switch from exhumation to deposition around this time.

3. Supergene alunite ages suggest enrichment ended by ~ 14.6 Ma at Cerro Colorado (Bouzari & Clark, 2002) and ~ 21 Ma at Spence (Rowland & Clark, 2001), whereas hematite precipitation at both deposits persisted into the Pleistocene. Post-hyperaridity hematite precipitation suggests weathering profiles continue to develop after the end of supergene enrichment—therefore hematite ages are not necessarily indicative of periods of enrichment.
4. Fluid isotopic compositions show deep formation water was present during hematite precipitation at Spence. Long-range groundwater recharge and the low-relief setting of Spence maintained a relatively shallow water table despite hyperaridity. Conversely, Cerro Colorado has been more susceptible to water table decay linked to aridity-induced canyon incision in the Precordillera. These results are consistent with models of groundwater recharge in the Atacama, within different morphotectonic settings (Houston 2002; Magaritz et al. 1990).

Both Spence and Cerro Colorado are enriched, yet there has been no canyon incision local to Spence, and incision of the Quebrada de Parca at Cerro Colorado began ~ 3.5 Myr after the apparent end of supergene enrichment. We suggest that exhumation-driven relative water table descent, rather than incision-driven water table decay, has been more important for the propagation of weathering fronts during supergene enrichment of both PCDs. Therefore, deeply exhumed areas (tectonic control) are more likely to host supergene enrichment than incised areas (climatic and/or tectonic control), unless incision occurred while conditions were conducive to copper leaching (prior to climate desiccation). The greater importance of exhumation, compared to canyon incision, is also demonstrated by the potential magnitude of each process. The cumulative thickness of rock which can be exposed above the water table through exhumation is on the order of kilometers (bringing PCDs from their depth of emplacement to the surface), whereas canyon incision can only exert a second-order control on the water table, over a smaller depth range. It appears that climate variability alone is insufficient to produce relative water table descent over the depth range recorded by weathering profiles in the Atacama.

Data Availability Statement

Data reported in this paper can be accessed at the BGS NGDC repository. Data reported in Cooper et al. (2016) can be accessed at the GSA repository: https://gsapubs.figshare.com/articles/journal_contribution/Supplemental_material_Aridity-induced_Miocene_canyon_incision_in_the_Central_Andes/12533894.

Acknowledgments

This work was funded by a NERC GW4+ UK DTP Studentship (NE/L002434/1) with CASE support from BHP. Additional funding for the (U-Th-Sm)/He work was provided by a Student Research Grant from SEG (SRG18-104; J. Shaw) and a Royal Society Grant (RG140683; F. Cooper). Isotopic analyses were supported by a NERC Isotope Geosciences Facilities Grant (IP-1752-1117; F. Cooper). The authors are grateful to BHP for permitting mine visits, Ed Bunker for sample collection, and Guillermo Santos, Reinaldo Guzman, and Lia Ituarte for advice and logistical assistance. The authors thank Martin Smith for feedback on a draft manuscript and Mark Cuthbert for discussion on water tables. The authors thank Pete Reiners and Carlos Marquardt for their constructive reviews, and Peter van der Beek for his editorial handling.

References

- Ague, J. J., & Brimhall, G. H. (1989). Geochemical modelling of steady state fluid flow and chemical reaction during supergene enrichment of porphyry copper deposits. *Economic Geology*, 84(3), 506–528. <https://doi.org/10.2113/gsecongeo.84.3.506>
- Alpers, C. N., & Brimhall, G. H. (1988). Middle Miocene climatic change in the Atacama Desert, northern Chile: Evidence from supergene mineralization at La Escondida. *Geological Society of America Bulletin*, 100(10), 1640–1656. [https://doi.org/10.1130/0016-7606\(1988\)100<1640:mmccit>2.3.co;2](https://doi.org/10.1130/0016-7606(1988)100<1640:mmccit>2.3.co;2)
- Amundson, R., Dietrich, W., Bellugi, D., Ewing, S., Nishiizumi, K., Chong, G., et al. (2012). Geomorphologic evidence for the late Pliocene onset of hyperaridity in the Atacama Desert. *Bulletin*, 124(7–8), 1048–1070. <https://doi.org/10.1130/b30445.1>
- Anderson, J. A. (1982). Characteristics of leached capping and techniques of appraisal. In S. R. Titley (Ed.), *Advances in geology of the porphyry copper deposits, southwestern North America* (pp. 275–296). University of Arizona Press.
- Arancibia, G., Matthews, S. J., & de Arce, C. P. (2006). K–Ar and $^{40}\text{Ar}/^{39}\text{Ar}$ geochronology of supergene processes in the Atacama Desert, Northern Chile: Tectonic and climatic relations. *Journal of the Geological Society*, 163(1), 107–118. <https://doi.org/10.1144/0016-764904-161>
- Aravena, R., Suzuki, O., Pena, H., Pollastri, A., Fuenzalida, H., & Grilli, A. (1999). Isotopic composition and origin of the precipitation in Northern Chile. *Applied Geochemistry*, 14(4), 411–422. [https://doi.org/10.1016/S0883-2927\(98\)00067-5](https://doi.org/10.1016/S0883-2927(98)00067-5)
- Armijo, R., Lacassin, R., Coudurier-Curveur, A., & Carrizo, D. (2015). Coupled tectonic evolution of Andean orogeny and global climate. *Earth-Science Reviews*, 143, 1–35. <https://doi.org/10.1016/j.earscirev.2015.01.005>
- Bähr, R., Lippolt, H. J., & Wernicke, R. S. (1994). Temperature-induced ^4He degassing of specularite and botryoidal hematite: A ^4He retention study. *Journal of Geophysical Research*, 99(B9), 17695–17707. <https://doi.org/10.1029/94jb01055>
- Bao, H., & Koch, P. L. (1999). Oxygen isotope fractionation in ferric oxide-water systems: Low temperature synthesis. *Geochimica et Cosmochimica Acta*, 63(5), 599–613. [https://doi.org/10.1016/S0016-7037\(99\)00005-8](https://doi.org/10.1016/S0016-7037(99)00005-8)
- Barnes, J. B., & Ehlers, T. A. (2009). End member models for Andean Plateau uplift. *Earth-Science Reviews*, 97(1–4), 105–132. <https://doi.org/10.1016/j.earscirev.2009.08.003>
- Bish, D. L., & Post, J. E. (Eds.). (2018). Modern powder diffraction (Vol. 20). Walter de Gruyter GmbH & Co KG.

- Bissig, T., & Riquelme, R. (2009). Contrasting landscape evolution and development of supergene enrichment in the El Salvador porphyry Cu and Potrerillos-El Hueso Cu-Au districts, northern Chile. In S. Titley (Ed.), *Supergene environments, processes and products* (Vol. 14, pp. 59–68). Society of Economic Geologists Special Publication.
- Blanco, N., Ladino, M., & Tomlinson, A. J. (2012). Geological Map of Mamiña, Tarapacá region (Vol. 1). National Geology Service and Regional Government of Tarapacá.
- Bookhagen, B., & Strecker, M. R. (2012). Spatiotemporal trends in erosion rates across a pronounced rainfall gradient: Examples from the southern Central Andes. *Earth and Planetary Science Letters*, 327, 97–110. <https://doi.org/10.1016/j.epsl.2012.02.005>
- Bouzari, F., & Clark, A. H. (2002). Anatomy, evolution, and metallogenic significance of the supergene orebody of the Cerro Colorado porphyry copper deposit, I Región, northern Chile. *Economic Geology*, 97(8), 1701–1740. <https://doi.org/10.2113/gsecongeo.97.8.1701>
- Brimhall, G. H., Alpers, C. N., & Cunningham, A. B. (1985). Analysis of supergene ore-forming processes and ground-water solute transport using mass balance principles. *Economic Geology*, 80(5), 1227–1256. <https://doi.org/10.2113/gsecongeo.80.5.1227>
- Cameron, E. M., & Leybourne, M. I. (2005). Relationship between groundwater chemistry and soil geochemical anomalies at the Spence copper porphyry deposit, Chile. *Geochemistry: Exploration, Environment, Analysis*, 5(2), 135–145. <https://doi.org/10.1144/1467-7873/03-064>
- Cameron, E. M., Leybourne, M. I., & Palacios, C. (2007). Atacamite in the oxide zone of copper deposits in northern Chile: Involvement of deep formation waters? *Mineralium Deposita*, 42(3), 205–218. <https://doi.org/10.1007/s00126-006-0108-0>
- Chávez, W. (2000). Supergene oxidation of copper deposits: Zoning and distribution of copper oxide minerals. *SEG Newsletter, Society of Economic Geologists*, 41, 10–21.
- Cooper, F. J., Adams, B. A., Blundy, J. D., Farley, K. A., McKeon, R. E., & Ruggiero, A. (2016). Aridity-induced Miocene canyon incision in the Central Andes. *Geology*, 44(8), 675–678. <https://doi.org/10.1130/g38254.1>
- Cruise, M. D., Boyce, A. J., & Fallick, A. E. (1999). Iron-oxide alteration associated with the carbonate-hosted Tynagh and Crinkill base-metal deposits, Ireland: Evidence for the involvement of dissolved atmospheric oxygen. *Society for geology applied to mineral deposits, abstracts with programs* (pp. 833–836).
- Das, S., Hendry, M. J., & Essilfie-Dughan, J. (2011). Transformation of two-line ferrihydrite to goethite and hematite as a function of pH and temperature. *Environmental Science & Technology*, 45(1), 268–275. <https://doi.org/10.1021/es101903y>
- Davis, W. L., de Pater, I., & McKay, C. P. (2010). Rain infiltration and crust formation in the extreme arid zone of the Atacama Desert, Chile. *Planetary and Space Science*, 58(4), 616–622. <https://doi.org/10.1016/j.pss.2009.08.011>
- Deng, X. D., Li, J. W., & Shuster, D. L. (2017). Late Mio-Pliocene chemical weathering of the Yulong porphyry Cu deposit in the eastern Tibetan Plateau constrained by goethite (U–Th)/He dating: Implication for Asian summer monsoon. *Earth and Planetary Science Letters*, 472, 289–298. <https://doi.org/10.1016/j.epsl.2017.04.043>
- Dold, B. (2003). *Enrichment processes in oxidizing sulfide mine tailings*. SGA News.
- Dunai, T. J., López, G. A. G., & Juez-Larré, J. (2005). Oligocene–Miocene age of aridity in the Atacama Desert revealed by exposure dating of erosion-sensitive landforms. *Geology*, 33(4), 321–324. <https://doi.org/10.1130/g21184.1>
- Enders, M. S., Knickerbocker, C., Titley, S. R., & Southam, G. (2006). The role of bacteria in the supergene environment of the Morenci porphyry copper deposit, Greenlee County, Arizona. *Economic Geology*, 101(1), 59–70. <https://doi.org/10.2113/gsecongeo.101.1.59>
- Evenstar, L. A., Mather, A. E., & Hartley, A. J. (2020). Using spatial patterns of fluvial incision to constrain continental-scale uplift in the Andes. *Global and Planetary Change*, 186, 103119. <https://doi.org/10.1016/j.gloplacha.2020.103119>
- Evenstar, L. A., Mather, A. E., Hartley, A. J., Stuart, F. M., Sparks, R. S. J., & Cooper, F. J. (2017). Geomorphology on geologic timescales: Evolution of the late Cenozoic Pacific paleosurface in Northern Chile and Southern Peru. *Earth-Science Reviews*, 171, 1–27. <https://doi.org/10.1016/j.earscirev.2017.04.004>
- Fariás, M., Charrier, R., Comte, D., Martinod, J., & Hérail, G. (2005). Late Cenozoic deformation and uplift of the western flank of the Altiplano: Evidence from the depositional, tectonic, and geomorphologic evolution and shallow seismic activity (northern Chile at 19°30'S). *Tectonics*, 24(4). <https://doi.org/10.1029/2004tc001667>
- Farley, K. A. (2002). (U–Th)/He dating: Techniques, calibrations, and applications. *Reviews in Mineralogy and Geochemistry*, 47(1), 819–844. <https://doi.org/10.2138/rmg.2002.47.18>
- Farley, K. A. (2018). Helium diffusion parameters of hematite from a single-diffusion-domain crystal. *Geochimica et Cosmochimica Acta*, 231, 117–129. <https://doi.org/10.1016/j.gca.2018.04.005>
- Farley, K. A., & Flowers, R. M. (2012). (U–Th)/Ne and multidomain (U–Th)/He systematics of a hydrothermal hematite from eastern Grand Canyon. *Earth and Planetary Science Letters*, 359, 131–140. <https://doi.org/10.1016/j.epsl.2012.10.010>
- Fritz, P., Suzuki, O., Silva, C., & Salati, E. (1981). Isotope hydrology of groundwaters in the Pampa del Tamarugal, Chile. *Journal of Hydrology*, 53(1–2), 161–184. [https://doi.org/10.1016/0022-1694\(81\)90043-3](https://doi.org/10.1016/0022-1694(81)90043-3)
- García, M., Gardeweg, M., Clavero, J., & Hérail, G. (2004). Sheet Arica, Tarapacá Region: National Geology and Mining Service. *Chile Geological Chart, Basic Geology Series*, 84, 1: 250,000 scale map.
- García, M., Riquelme, R., Fariás, M., Hérail, G., & Charrier, R. (2011). Late Miocene–Holocene canyon incision in the western Altiplano, northern Chile: Tectonic or climatic forcing? *Journal of the Geological Society*, 168(4), 1047–1060. <https://doi.org/10.1144/0016-76492010-134>
- Garreaud, R. D., Molina, A., & Fariás, M. (2010). Andean uplift, ocean cooling and Atacama hyperaridity: A climate modeling perspective. *Earth and Planetary Science Letters*, 292(1–2), 39–50. <https://doi.org/10.1016/j.epsl.2010.01.017>
- Giuliani, G., Fallick, A. E., Garnier, V., France-Lanord, C., Ohnenstetter, D., & Schwarz, D. (2005). Oxygen isotope composition as a tracer for the origins of rubies and sapphires. *Geology*, 33(4), 249–252. <https://doi.org/10.1130/g21261.1>
- Hartley, A. J., & May, G. (1998). Miocene gypcetes from the Calama Basin, northern Chile. *Sedimentology*, 45(2), 351–364. <https://doi.org/10.1046/j.1365-3091.1998.0166e.x>
- Hartley, A. J., & Rice, C. M. (2005). Controls on supergene enrichment of porphyry copper deposits in the Central Andes: A review and discussion. *Mineralium Deposita*, 40(5), 515–525. <https://doi.org/10.1007/s00126-005-0017-7>
- Heim, J. A., Vasconcelos, P. M., Shuster, D. L., Farley, K. A., & Broadbent, G. (2006). Dating paleochannel iron ore by (U–Th)/He analysis of supergene goethite, Hamersley province, Australia. *Geology*, 34(3), 173–176. <https://doi.org/10.1130/g22003.1>
- Hofmann, F., Reichenbacher, B., & Farley, K. A. (2017). Evidence for >5 Ma paleo-exposure of an Eocene–Miocene paleosol of the Bohnernz Formation, Switzerland. *Earth and Planetary Science Letters*, 465, 168–175. <https://doi.org/10.1016/j.epsl.2017.02.042>
- Hofmann, F., Treffkorn, J., & Farley, K. A. (2020). U-loss associated with laser-heating of hematite and goethite in vacuum during (U–Th)/He dating and prevention using high O₂ partial pressure. *Chemical Geology*, 532, 119350. <https://doi.org/10.1016/j.chemgeo.2019.119350>
- Hoke, G. D., Isacks, B. L., Jordan, T. E., Blanco, N., Tomlinson, A. J., & Ramezani, J. (2007). Geomorphic evidence for post-10 Ma uplift of the western flank of the central Andes 18°30'–22°S. *Tectonics*, 26(5). <https://doi.org/10.1029/2006tc002082>

- Hoke, G. D., Isacks, B. L., Jordan, T. E., & Yu, J. S. (2004). Groundwater-sapping origin for the giant quebradas of northern Chile. *Geology*, 32(7), 605–608. <https://doi.org/10.1130/g20601.1>
- Hollingworth, S. E. (1964). Dating the uplift of the Andes of northern Chile. *Nature*, 201(4914), 17–20. <https://doi.org/10.1038/201017a0>
- House, M. A., Farley, K. A., & Stockli, D. (2000). Helium chronometry of apatite and titanite using Nd-YAG laser heating. *Earth and Planetary Science Letters*, 183(3–4), 365–368. [https://doi.org/10.1016/S0012-821X\(00\)00286-7](https://doi.org/10.1016/S0012-821X(00)00286-7)
- Houston, J. (2002). Groundwater recharge through an alluvial fan in the Atacama Desert, northern Chile: Mechanisms, magnitudes and causes. *Hydrological Processes*, 16(15), 3019–3035. <https://doi.org/10.1002/hyp.1086>
- Houston, J. (2006a). Evaporation in the Atacama Desert: An empirical study of spatio-temporal variations and their causes. *Journal of Hydrology*, 330(3–4), 402–412. <https://doi.org/10.1016/j.jhydrol.2006.03.036>
- Houston, J. (2006b). Variability of precipitation in the Atacama Desert: Its causes and hydrological impact. *International Journal of Climatology: A Journal of the Royal Meteorological Society*, 26(15), 2181–2198. <https://doi.org/10.1002/joc.1359>
- Houston, J. (2009). A recharge model for high altitude, arid, Andean aquifers. *Hydrological Processes: An International Journal*, 23(16), 2383–2393. <https://doi.org/10.1002/hyp.7350>
- Houston, J., & Hartley, A. J. (2003). The central Andean west-slope rainshadow and its potential contribution to the origin of hyper-aridity in the Atacama Desert. *International Journal of Climatology: A Journal of the Royal Meteorological Society*, 23(12), 1453–1464. <https://doi.org/10.1002/joc.938>
- Jayne, R. S., Pollyea, R. M., Dodd, J. P., Olson, E. J., & Swanson, S. K. (2016). Spatial and temporal constraints on regional-scale groundwater flow in the Pampa del Tamarugal Basin, Atacama Desert, Chile. *Hydrogeology Journal*, 24(8), 1921–1937. <https://doi.org/10.1007/s10040-016-1454-3>
- Jordan, T., Lameli, C. H., Kirk-Lawlor, N., & Godfrey, L. (2015). Architecture of the aquifers of the Calama Basin, Loa catchment basin, northern Chile. *Geosphere*, 11(5), 1438–1474. <https://doi.org/10.1130/ges01176.1>
- Jordan, T. E., Kirk-Lawlor, N. E., Blanco, N. P., Rech, J. A., & Cosentino, N. J. (2014). Landscape modification in response to repeated onset of hyperarid paleoclimate states since 14 Ma, Atacama Desert, Chile. *GSA Bulletin*, 126(7–8), 1016–1046. <https://doi.org/10.1130/b30978.1>
- Jordan, T. E., Nester, P. L., Blanco, N., Hoke, G. D., Dávila, F., & Tomlinson, A. J. (2010). Uplift of the Altiplano-Puna plateau: A view from the west. *Tectonics*, 29(5). <https://doi.org/10.1029/2010tc002661>
- Ketcham, R. A., Gautheron, C., & Tassan-Got, L. (2011). Accounting for long alpha-particle stopping distances in (U-Th-Sm)/He geochronology: Refinement of the baseline case. *Geochimica et Cosmochimica Acta*, 75(24), 7779–7791. <https://doi.org/10.1016/j.gca.2011.10.011>
- Lichtner, P. C., & Biino, G. G. (1992). A first principles approach to supergene enrichment of a porphyry copper protore: I. Cu-Fe-S subsystem. *Geochimica et Cosmochimica Acta*, 56(11), 3987–4013. [https://doi.org/10.1016/0016-7037\(92\)90012-8](https://doi.org/10.1016/0016-7037(92)90012-8)
- Lippolt, H. J., Wernicke, R. S., & Boschmann, W. (1993). ⁴He diffusion in specular hematite. *Physics and Chemistry of Minerals*, 20(6), 415–418. <https://doi.org/10.1007/bf00203111>
- Magaritz, M., Aravena, R., Peña, H., Suzuki, O., & Grilli, A. (1990). Source of ground water in the deserts of northern Chile: Evidence of deep circulation of ground water from the Andes. *Groundwater*, 28(4), 513–517. <https://doi.org/10.1111/j.1745-6584.1990.tb01706.x>
- Marshall, T. A., Morris, K., Law, G. T., Livens, F. R., Mosselmans, J. F. W., Bots, P., & Shaw, S. (2014). Incorporation of uranium into hematite during crystallization from ferrihydrite. *Environmental Science & Technology*, 48(7), 3724–3731. <https://doi.org/10.1021/es500212a>
- May, G., Hartley, A. J., Chong, G., Stuart, F., Turner, P., & Kape, S. J. (2005). Eocene to Pleistocene lithostratigraphy, chronostratigraphy and tectono-sedimentary evolution of the Calama Basin, northern Chile. *Andean Geology*, 32(1), 33–58.
- McBriarty, M. E., Kerisit, S., Bylaska, E. J., Shaw, S., Morris, K., & Ilton, E. S. (2018). Iron vacancies accommodate uranyl incorporation into hematite. *Environmental Science & Technology*, 52(11), 6282–6290. <https://doi.org/10.1021/acs.est.8b00297>
- Miller, H. B., Vasconcelos, P. M., Eiler, J. M., & Farley, K. A. (2017). A Cenozoic terrestrial paleoclimate record from He dating and stable isotope geochemistry of goethites from Western Australia. *Geology*, 45(10), 895–898. <https://doi.org/10.1130/g38989.1>
- Monteiro, H. S., Vasconcelos, P. M. P., & Farley, K. A. (2018). A combined (U-Th)/He and cosmogenic ³He record of landscape armoring by biogeochemical iron cycling. *Journal of Geophysical Research: Earth Surface*, 123(2), 298–323. <https://doi.org/10.1002/2017jfr004282>
- Monteiro, H. S., Vasconcelos, P. M. P., Farley, K. A., & Lopes, C. A. M. (2018). Age and evolution of diachronous erosion surfaces in the Amazon: Combining (U-Th)/He and cosmogenic ³He records. *Geochimica et Cosmochimica Acta*, 229, 162–183. <https://doi.org/10.1016/j.gca.2018.02.045>
- Monteiro, H. S., Vasconcelos, P. M. P., Farley, K. A., Spier, C. A., & Mello, C. L. (2014). (U-Th)/He geochronology of goethite and the origin and evolution of cangas. *Geochimica et Cosmochimica Acta*, 131, 267–289. <https://doi.org/10.1016/j.gca.2014.01.036>
- Mpodozis, C., & Cornejo, P. (2012). Cenozoic tectonics and porphyry copper systems of the Chilean Andes. In J. W. Hedenquist, M. Harris, & F. Camus (Eds.), *Geology and genesis of major copper deposits and districts of the world. A tribute to Richard H. Sillitoe*. Society of Economic Geologists. <https://doi.org/10.5382/sp.16.14>
- Palacios, C., Ramírez, L. E., Townley, B., Solari, M., & Guerra, N. (2007). The role of the Antofagasta-Calama Lineament in ore deposit deformation in the Andes of northern Chile. *Mineralium Deposita*, 42(3), 301–308. <https://doi.org/10.1007/s00126-006-0113-3>
- Pidgeon, R. T., Brander, T., & Lippolt, H. J. (2004). Late Miocene (U+Th)/⁴He ages of ferruginous nodules from lateritic duricrust, Darling Range, Western Australia. *Australian Journal of Earth Sciences*, 51(6), 901–909. <https://doi.org/10.1111/j.1400-0952.2004.01094.x>
- Quade, J., Rasbury, E. T., Huntington, K. W., Hudson, A. M., Vonhof, H., Anchukaitis, K., et al. (2017). Isotopic characterization of late Neogene travertine deposits at Barrancas Blancas in the eastern Atacama Desert, Chile. *Chemical Geology*, 466, 41–56. <https://doi.org/10.1016/j.chemgeo.2017.05.004>
- Rech, J. A., Currie, B. S., Jordan, T. E., Riquelme, R., Lehmann, S. B., Kirk-Lawlor, N. E., et al. (2019). Massive middle Miocene gypsic paleosols in the Atacama Desert and the formation of the Central Andean rain-shadow. *Earth and Planetary Science Letters*, 506, 184–194. <https://doi.org/10.1016/j.epsl.2018.10.040>
- Rech, J. A., Currie, B. S., Shullenberger, E. D., Dunagan, S. P., Jordan, T. E., Blanco, N., et al. (2010). Evidence for the development of the Andean rain shadow from a Neogene isotopic record in the Atacama Desert, Chile. *Earth and Planetary Science Letters*, 292(3–4), 371–382. <https://doi.org/10.1016/j.epsl.2010.02.004>
- Reich, M., Palacios, C., Parada, M. A., Fehn, U., Cameron, E. M., Leybourne, M. I., & Zúñiga, A. (2008). Atacamite formation by deep saline waters in copper deposits from the Atacama Desert, Chile: Evidence from fluid inclusions, groundwater geochemistry, TEM, and ³⁶Cl data. *Mineralium Deposita*, 43(6), 663–675. <https://doi.org/10.1007/s00126-008-0184-4>
- Reich, M., Palacios, C., Vargas, G., Luo, S., Cameron, E. M., Leybourne, M. I., et al. (2009). Supergene enrichment of copper deposits since the onset of modern hyperaridity in the Atacama Desert, Chile. *Mineralium Deposita*, 44(5), 497–504. <https://doi.org/10.1007/s00126-009-0229-3>

- Reiners, P. W., Chan, M. A., & Evenson, N. S. (2014). (U-Th)/He geochronology and chemical compositions of diagenetic cement, concretions, and fracture-filling oxide minerals in Mesozoic sandstones of the Colorado Plateau. *GSA Bulletin*, 126(9–10), 1363–1383. <https://doi.org/10.1130/b30983.1>
- Richards, J. P. (2013). Giant ore deposits formed by optimal alignments and combinations of geological processes. *Nature Geoscience*, 6(11), 911–916. <https://doi.org/10.1038/ngeo1920>
- Riffel, S. B., Vasconcelos, P. M., Carmo, I. O., & Farley, K. A. (2016). Goethite (U-Th)/He geochronology and precipitation mechanisms during weathering of basalts. *Chemical Geology*, 446, 18–32. <https://doi.org/10.1016/j.chemgeo.2016.03.033>
- Riquelme, R., Hérail, G., Martinod, J., Charrier, R., & Darrozes, J. (2007). Late Cenozoic geomorphologic signal of Andean forearc deformation and tilting associated with the uplift and climate changes of the Southern Atacama Desert (26°S–28°S). *Geomorphology*, 86(3–4), 283–306. <https://doi.org/10.1016/j.geomorph.2006.09.004>
- Riquelme, R., Tapia, M., Campos, E., Mpodozis, C., Carretier, S., González, R., et al. (2018). Supergene and exotic Cu mineralization occur during periods of landscape stability in the Centinela Mining District, Atacama Desert. *Basin Research*, 30(3), 395–425. <https://doi.org/10.1111/bre.12258>
- Ritter, B., Binnie, S. A., Stuart, F. M., Wennrich, V., & Dunai, T. J. (2018). Evidence for multiple Plio-Pleistocene lake episodes in the hyper-arid Atacama Desert. *Quaternary Geochronology*, 44, 1–12. <https://doi.org/10.1016/j.quageo.2017.11.002>
- Rowland, M., & Clark, A. H. (2001). Temporal overlap of supergene alteration and high-sulfidation mineralization in the Spence porphyry copper deposit, II Región, Chile [abs.]. In Geological Society of America, Abstracts with Programs (Vol. 33).
- Sanchez, C., Brichau, S., Riquelme, R., Carretier, S., Bissig, T., Lopez, C., et al. (2018). Exhumation history and timing of supergene copper mineralisation in an arid climate: New thermochronological data from the Centinela District, Atacama, Chile. *Terra Nova*, 30(1), 78–85. <https://doi.org/10.1111/ter.12311>
- Scanlon, B. R., Keese, K. E., Flint, A. L., Flint, L. E., Gaye, C. B., Edmunds, W. M., & Simmers, I. (2006). Global synthesis of groundwater recharge in semiarid and arid regions. *Hydrological Processes: An International Journal*, 20(15), 3335–3370. <https://doi.org/10.1002/hyp.6335>
- Scheiing, K. W., Moya, C. E., & Tröger, U. (2017). Insights into Andean slope hydrology: Reservoir characteristics of the thermal Pica spring system, Pampa del Tamarugal, northern Chile. *Hydrogeology Journal*, 25(6), 1833–1852. <https://doi.org/10.1007/s10040-017-1533-0>
- Schlunegger, F., Zeilinger, G., Kounov, A., Kober, F., & Hüsner, B. (2006). Scale of relief growth in the forearc of the Andes of Northern Chile (Arica latitude, 18°S). *Terra Nova*, 18(3), 217–223. <https://doi.org/10.1111/j.1365-3121.2006.00682.x>
- Shuster, D. L., Farley, K. A., Vasconcelos, P. M., Balco, G., Monteiro, H. S., Waltenberg, K., & Stone, J. O. (2012). Cosmogenic ³He in hematite and goethite from Brazilian “canga” duricrust demonstrates the extreme stability of these surfaces. *Earth and Planetary Science Letters*, 329, 41–50. <https://doi.org/10.1016/j.epsl.2012.02.017>
- Sillitoe, R. H. (2005). Supergene oxidized and enriched porphyry copper and related deposits. *Economic Geology*, 100, 723–768. <https://doi.org/10.5382/av100.22>
- Sillitoe, R. H. (2010). Porphyry copper systems. *Economic Geology*, 105(1), 3–41. <https://doi.org/10.2113/gsecongeo.105.1.3>
- Sillitoe, R. H., & McKee, E. H. (1996). Age of supergene oxidation and enrichment in the Chilean porphyry copper province. *Economic Geology*, 91(1), 164–179. <https://doi.org/10.2113/gsecongeo.91.1.164>
- Sultan, K. (2015). Stable oxygen and hydrogen isotope fractionation factors for the Goethite (hematite)-water system. *Oriental Journal of Chemistry*, 31(1), 69–75. <https://doi.org/10.13005/ojc/310107>
- Sun, T., Bao, H., Reich, M., & Hemming, S. R. (2018). More than ten million years of hyper-aridity recorded in the Atacama Gravels. *Geochimica et Cosmochimica Acta*, 227, 123–132. <https://doi.org/10.1016/j.gca.2018.02.021>
- Toth, J. (1963). A theoretical analysis of groundwater flow in small drainage basins. *Journal of Geophysical Research*, 68(16), 4795–4812. <https://doi.org/10.1029/jz068i016p04795>
- Tsang, D. P., Wallis, S. R., Yamamoto, K., Takeuchi, M., Hidaka, H., Horie, K., & Tattitch, B. C. (2018). Zircon U–Pb geochronology and geochemistry of the Cerro Colorado porphyry copper deposit, northern Chile. *Ore Geology Reviews*, 93, 114–140. <https://doi.org/10.1016/j.oregeorev.2017.12.019>
- Vasconcelos, P. M. (1999). K–Ar and ⁴⁰Ar/³⁹Ar geochronology of weathering processes. *Annual Review of Earth and Planetary Sciences*, 27(1), 183–229. <https://doi.org/10.1146/annurev.earth.27.1.183>
- Vasconcelos, P. M., Heim, J. A., Farley, K. A., Monteiro, H., & Waltenberg, K. (2013). ⁴⁰Ar/³⁹Ar and (U–Th)/He–⁴He/³He geochronology of landscape evolution and channel iron deposit genesis at Lynn Peak, Western Australia. *Geochimica et Cosmochimica Acta*, 117, 283–312. <https://doi.org/10.1016/j.gca.2013.03.037>
- Viguier, B., Jourde, H., Yáñez, G., Lira, E. S., Leonardi, V., Moya, C. E., et al. (2018). Multidisciplinary study for the assessment of the geometry, boundaries and preferential recharge zones of an overexploited aquifer in the Atacama Desert (Pampa del Tamarugal, Northern Chile). *Journal of South American Earth Sciences*, 86, 366–383. <https://doi.org/10.1016/j.jsames.2018.05.018>
- Yapp, C. J. (1987). Oxygen and hydrogen isotope variations among goethites (α-FeOOH) and the determination of paleotemperatures. *Geochimica et Cosmochimica Acta*, 51(2), 355–364. [https://doi.org/10.1016/0016-7037\(87\)90247-x](https://doi.org/10.1016/0016-7037(87)90247-x)
- Yapp, C. J. (1990). Oxygen isotopes in iron (III) oxides: 1. Mineral-water fractionation factors. *Chemical Geology*, 85(3–4), 329–335. [https://doi.org/10.1016/0009-2541\(90\)90010-5](https://doi.org/10.1016/0009-2541(90)90010-5)
- Yapp, C. J. (2000). Climatic implications of surface domains in arrays of δD and δ¹⁸O from hydroxyl minerals: Goethite as an example. *Geochimica et Cosmochimica Acta*, 64(12), 2009–2025. [https://doi.org/10.1016/S0016-7037\(00\)00347-1](https://doi.org/10.1016/S0016-7037(00)00347-1)
- Yapp, C. J. (2001). Rusty relics of Earth history: Iron (III) oxides, isotopes, and surficial environments. *Annual Review of Earth and Planetary Sciences*, 29(1), 165–199. <https://doi.org/10.1146/annurev.earth.29.1.165>
- Zheng, Y. F., & Simon, K. (1991). Oxygen isotope fractionation in hematite and magnetite: A theoretical calculation and application to geothermometry of metamorphic iron-formations. *European Journal of Mineralogy*, 3, 877–886. <https://doi.org/10.1127/ejm/3/5/0877>

Reference From the Supporting Information

- Clayton, R. N., & Epstein, S. (1961). The use of oxygen isotopes in high-temperature geological thermometry. *The Journal of Geology*, 69(4), 447–452. <https://doi.org/10.1086/626760>